Applied Ocean Research 170 (2026) 105045

Contents lists available at ScienceDirect

Applied Ocean Research

journal homepage: www.elsevier.com/locate/apor

Research paper

Probabilistic modelling of the armour damage of cube-armoured mound breakwaters along their design life using experimental data

P. Andrés-Wörz, O. Morales-Nápoles, P. Mares-Nasarre *

Faculty of Civil Engineering and Geosciences, Delft University of Technology, Delft, The Netherlands

ARTICLE INFO

Keywords:
Mound breakwater
Armour damage
Gamma process
Gaussian copula-based Bayesian Network
Damage progression

ABSTRACT

Field data of armour damage in mound breakwaters is scarce, and experimental testing methods usually neglect the influence of pre-existing damage on subsequent damage increments. This study proposes a probabilistic framework, based on a dataset of 44 cumulative damage experiments, to estimate long-term damage progression in a full-scale, non-overtopped, cube-armoured mound breakwater located in the depth-induced wave breaking zone. A Gaussian copula-based Bayesian network is constructed to model the multivariate relationships between existing armour damage (S_e), the increment of armour damage (ΔS_e), the dimensionless water depth at the toe of the structure (h_s/H_{m0}), wave steepness (H_{m0}/L_{0p}), and the stability number (N_s). Each variable is modelled with a univariate parametric distribution, enabling inference of probabilities for values not directly observed in the experimental dataset. Model validation includes testing the Gaussian copula assumption, which is deemed a reasonable model, and assessing the defined graph with satisfactory results. The model is conditionalized using a historical wave dataset to generate synthetic damage curves, which are subsequently used to quantify a gamma process to model the survivability of the structure along its design life. A case study of a hypothetical breakwater with $D_n = 2$ m close to the port of Tarragona (Spain) illustrates the methodology. According to the results of the model, the probability of observing a dimensionless damage $S_e > 5$ corresponding to Initiation of Destruction after 10 years is 0.29. Overall, the obtained results are deemed conservative; this could be caused by the use of data from 2D experiments which do not take into account oblique wave attack. However, the approach is adaptable to other datasets with additional variables, breakwaters in different conditions or with other configurations, and can also be used in combination with simulations of synthetic wave data, making it relevant under changing climate conditions.

1. Introduction

Mound breakwaters play a critical role in protecting ports and coastal zones from waves and storms. Therefore, they are pivotal for the functioning of harbours and thereby the economic development of coastal regions (Haralambides, 2017). These structures are continually subjected to harsh environmental conditions, which can become increasingly extreme due to the effects of climate change (Vousdoukas et al., 2018; IPCC, 2023). In addition, many existing breakwaters are approaching or have surpassed their design life, raising concerns about their future performance and structural integrity (Medina, 2024). Therefore, further tools are needed to better assess the life cycle of these structures under changing loading conditions.

Hydraulic stability of the armour layer of mound breakwaters is considered one of the main failure modes during their design phase (Burcharth and Liu, 1995). This failure mode is driven by wave-induced forces that displace individual armour units. A major challenge in assessing the armour damage in mound breakwaters is the limited availability of reliable field data from port structures, particularly with respect to long-term damage progression and breakwater failure (Allsop et al., 2010). Recent advances in non-invasive and cost-effective monitoring techniques, such as aerial imagery (Henriques et al., 2024), LIDAR scanning (Puente et al., 2014), and automated visual inspection with 3D RGB-D cameras (Musumeci et al., 2018), are promising for improving data collection and monitoring of stability. However, it can take decades to observe meaningful levels of degradation. Laboratory experiments can overcome this limitation by enabling controlled testing under accelerated conditions. Consequently, traditional design of breakwaters has relied heavily on empirical or semi-empirical formulations derived from small-scale physical model tests (e.g. Hudson, 1959; van der Meer, 1987; USACE, 2002; CIRIA/CUR/CETMEF, 2007).

* Corresponding author.
E-mail addresses: p.andresworz@student.tudelft.nl (P. Andrés-Wörz), o.moralesnapoles@tudelft.nl (O. Morales-Nápoles), p.maresnasarre@tudelft.nl (P. Mares-Nasarre).

https://doi.org/10.1016/j.apor.2026.105045
Received 21 October 2025; Received in revised form 17 March 2026; Accepted 24 March 2026
Available online 1 April 2026

Specifically for double-layer randomly-placed cube-armours, recently empirical investigations have been performed on low-crested structures (Yuksel et al., 2025), on structures with high-density cubes (Yuksel et al., 2022) or berms in the front slope (Yuksel et al., 2020), and in depth-limited breaking wave conditions for non-overtopped (Mares-Nasarre et al., 2022) and overtopped structures (Mares-Nasarre et al., 2021).

A limitation of physical experiments is that the number of possible tests in an experimental campaign is finite, limiting the validity of the results to the tested experimental ranges. In addition, Scaravaglione et al. (2025b) pointed out that a significant uncertainty remains in experimental results that may arise from variability in incident wave conditions, structural characteristics (packing density or armour unit placement, between others) and damage quantification methodologies, as well as from scale effects when translating laboratory results to full-scale conditions. Given the uncertainties inherent in wave loading and structural response, probabilistic methods are increasingly introduced to model wave-structure interactions (e.g. Castillo et al., 2012; Mares-Nasarre et al., 2024b; Mares-Nasarre, 2025). These models allow to incorporate the randomness and uncertainty directly into the design processes.

Experiments on the hydraulic stability of the armour layer of mound breakwaters are usually conducted by accumulating damage of experiments with increasing wave heights (e.g. Mares-Nasarre et al., 2022; Herrera et al., 2017) or by rebuilding the structure after each test run (e.g. van Gent et al., 2003; Scaravaglione et al., 2025a). However, as Martín-Hidalgo et al. (2014) and Marzeddu et al. (2020) pointed out, damage evolution is also affected by the sequence of events in a storm. That is, the damage that the structure already presents when facing an incoming wave storm influences the damage that such a storm will produce on the breakwater (Castillo et al., 2012; Lira-Loarca et al., 2020). Thus, further research should address how laboratory data obtained with the usual experimental methods can be used to assess the long-term degradation of a full-scale breakwater over its lifetime.

Stochastic processes have been widely proposed to model infrastructure deterioration with the aim to support maintenance planning and decision-making. Markov models are the most common due to their assumption of independent increments and their simplicity (Norris, 1997). Markov processes can be either discrete-time (Markov chains) or continuous-time (e.g. Gamma process) processes. Armour damage deterioration is a continuous process in time, monotonic and irreversible, as the structure does not recover on its own after suffering damage. The gamma process has been proposed to model such type of processes, for instance for the erosive degradation of river groynes (Mares-Nasarre et al., 2024a) or the reduction of height in dikes along their lifetime (van Noortwijk, 2009). It is a continuous stochastic process in time with an infinite number of small, positive, monotonic jumps, making it suitable to model continuous degradation with random fluctuations. Other examples of its application are (cavitation) erosion (Chatenet et al., 2021), concrete creep (Cinlar et al., 1977) or crack growth (Guida and Penta, 2015).

Traditionally, these stochastic processes are quantified using multiple historical records of the evolution of degradation. However, since such data is scarce in mound breakwaters, it might be unavailable or insufficient, and if sufficient, it may not be representative of the future performance of the structure considering the current context of potentially changing climatic loadings. Therefore, there is a need for models that can generate historical damage records using laboratory data and use these to quantify a stochastic process, thereby incorporating uncertainty in both the damage evolution process and the influencing environmental factors. To the authors' knowledge, there is no such methodology for mound breakwaters in the scientific literature.

Bayesian Networks (BNs) have been widely used to model probabilistic relationships and deterioration (e.g. Straub, 2009) in the field of structural reliability. BNs are graphical models that represent conditional dependencies among variables and can incorporate both observed data and expert knowledge. Gaussian copula-based Bayesian Networks (GCBN) are continuous BNs that build the joint distribution in bivariate pieces using Gaussian copulas, thus separating the marginal distributions from their dependence structure (Hanea et al., 2006, 2015). The assumption of using Gaussian copulas is advantageous since it allows modelling high-dimensional systems at relatively low computational costs. Furthermore, once a GCBN is established, it is possible to estimate the distribution of a set of variables given the values of other variables are known through inference. Examples of the application of GCBNs in Civil Engineering are the modelling of the hydraulic boundary conditions during hurricane flood risk analysis in a coastal watershed (Sebastian et al., 2017), the characterization of the spatial variability of corrosion depths in ageing steel bridges (Barros et al., 2024), the modelling of weigh-in-motion loads in bridges (Mendoza-Lugo et al., 2022) and the estimation of the mean overtopping discharge on mound breakwaters (Mares-Nasarre, 2025).

This study aims to propose a probabilistic framework to generate synthetic damage curves of mound breakwaters quantified with laboratory data from cumulative damage experiments and that accounts for the dependence between the existing damage of the structure at a given time, the loading variables, and the produced increment of damage. These synthetic curves are later used to quantify a gamma process to assess the long-term survivability of the mound breakwater. To do so, a Gaussian copula-based Bayesian Network (GCBN) is proposed to model the joint distribution of the loading variables, the pre-existing damage in the armour, and the increment of damage generated by the loading variables. The GCBN allows for the generation of synthetic time series of damage that are later used to quantify the gamma process. This framework uses as input experimental data from physical model tests of cumulative damage of non-overtopped cube-armoured breakwaters in the depth-induced breaking zone reported in Mares-Nasarre et al. (2022). Therefore, the proposed framework can be applied to similar datasets in the literature (e.g. Herrera et al., 2017; Gómez-Martín and Medina, 2014). This paper has the following structure. Section 2 describes the experimental data used to develop the probabilistic model. Section 3 gives an overview of the proposed methodology. The model is constructed and validated in Section 4 and its application is shown using a case study of an idealized breakwater close to the port of Tarragona in Section 5. The results are discussed and conclusions are drawn in Section 6.

2. Dataset and selection of variables

This section describes the experimental data used to construct the probabilistic framework to model armour damage evolution and defines the explanatory variables used.

2.1. Description of experimental data

This research makes use of the physical model tests described in Mares-Nasarre et al. (2022) which were conducted in the wave flume of the Laboratory of Ports and Coasts at the Universitat Politècnica de València (LPC-UPV), measuring 30 m × 1.2 m × 1.2 m. Fig. 1 depicts the longitudinal cross-section of the LPC-UPV wave flume.

Experiments were carried out to assess the armour damage evolution of randomly-placed cube-armoured mound breakwaters. Fig. 2 shows the cross-section of the breakwater model. The model consists of a core (D_{n50} = 0.68 cm), a filter layer (D_{n50} = 1.78 cm), a rock toe berm (D_{n50} = 2.47 cm), and an armour layer comprising two layers of randomly-placed cube armour units (D_n = 3.97 cm) with an armour slope of $\cot\alpha = 3/2$ and an initial packing density of $\Phi_p = 1.18$. D_{n50} is the nominal stone diameter or equivalent cube size, whilst D_n is the nominal diameter of the armour unit ($D_n = M/\rho$ where M is the mass and ρ is the mass density of the rock).

Test series were conducted with different combinations of water depth at the toe of the structure (h_s) and wave steepness ($s_{0p} = H_{m0}/L_{0p}$, where $H_{m0} = 4(m_0)^{0.5}$ is the spectral significant wave height,

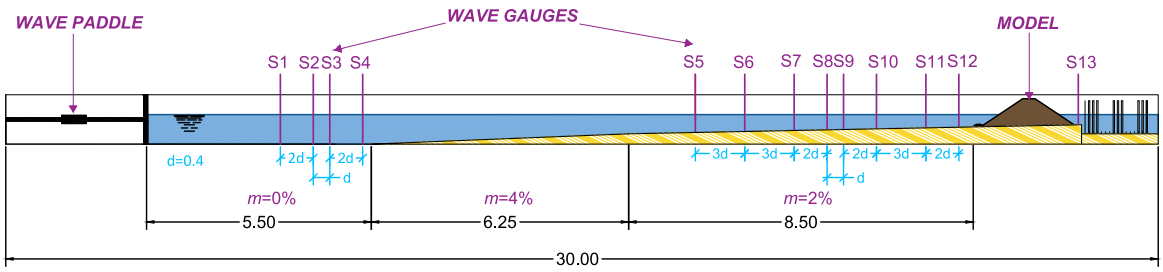

Fig. 1. Longitudinal cross-section of the wave flume (dimensions in metres), where m denotes the bottom slope.

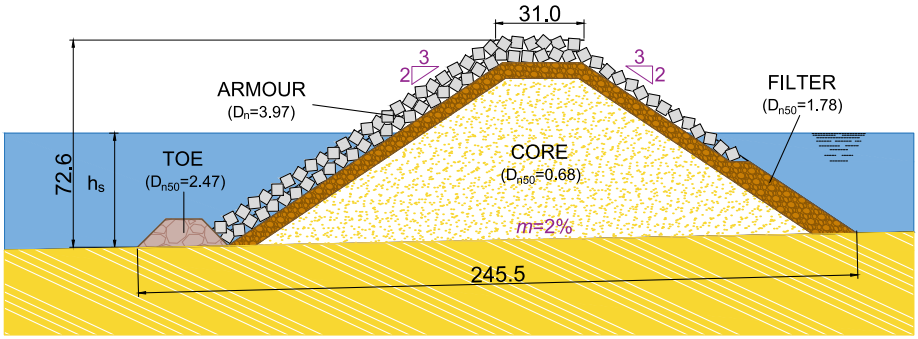

Fig. 2. Cross-section of the tested mound breakwater model (dimensions in centimetres), where D_n and D_{n50} are the nominal diameter of the armour unit and stones, respectively, and h_s is the water depth at the toe of the structure.

m_0 is the zeroth-order spectral moment, $L_{0p} = gT_p^2/2\pi$ is the deep-water wave length, g is the gravitational acceleration, and T_p is the peak wave period): h_s(m) = 0.2 with s_{0p} = 0.02 & 0.05; h_s(m) = 0.3 with s_{0p} = 0.02, 0.03 & 0.05; and h_s(m) = 0.4 with s_{0p} = 0.05. In each series, tests were started with H_{m0} in the wave generation zone of approximately 8 cm that generated no damage to the structure. H_{m0} in the wave generation zone was increased in increments of 1 cm between test runs. Tests were stopped when initiation of destruction occurred or wave breaking took place in the wave generation zone. Each test run consisted of 1000 random waves generated following a JONSWAP spectrum ($\gamma = 3.3$). After each test run, the armour damage was quantified.

Thirteen wave gauges were placed at various positions along the wave flume to measure the surface elevation, as shown in Fig. 1. S1–S4 were placed in the wave generation zone to separate incident and reflected waves; S5–S12 were located near the model; and S13 was placed behind the model to observe the water level at the rear side. Since it is not possible to separate incident and reflected waves in the depth-induced breaking zone, the SwanOne model was applied to estimate wave characteristics (T_p and H_{m0}) at a distance of $3h_s$ from the structure, following recommendations by Herrera et al. (2017).

In Mares-Nasarre et al. (2022), the armour damage was quantified using the dimensionless armour damage parameter (S_e), as defined by Broderick (1983):

$$S_e = \frac{A_e}{D_{n50}^2} \tag{1}$$

where A_e is the eroded area. A_e was calculated using the Virtual Net method proposed by Gómez-Martín and Medina (2006). In this method, the upper layer is divided into strips of a constant width and length. The damage in each strip (S_i) is calculated and then S_i is integrated over the entire slope. The Virtual Net method accounts for damage generated from both the extraction of armour units and changes in the armour porosity such as Heterogeneous Packing (HeP). HeP refers to the failure mode caused due to the packing density of the armour layer being reduced near and above the mean water level and increased below it (Gómez-Martín and Medina, 2014). This mechanism is particularly relevant for cube armour units due to their preferred face-to-face orientation (Mares-Nasarre et al., 2022). Photographs were taken before and after each test run to document the damage.

In addition to the quantitative description of armour damage, Mares-Nasarre et al. (2022) also characterized the damage qualitatively following the four qualitative damage levels for double-layer mound breakwaters defined in Losada et al. (1986) and Vidal et al. (1991), being:

1. **Initiation of Damage (IDa):** a few armour units are removed from the upper layer and holes of approximately the size of a single armour unit become visible;
2. **Initiation of Iribarren Damage (IIDa):** a large area of the upper layer is damaged and therefore units from the bottom layer start to be lost;
3. **Initiation of Destruction (IDe):** the filter layers becomes visible due to extraction of elements from the bottom layer;
4. **Destruction (De):** elements are removed from the filter layer.

Mares-Nasarre et al. (2022) quantified the corresponding levels of damage for this dataset and found that $S_e(IDa) \approx 0.6$, $S_e(IIDa) \approx 1.7$ and $S_e(IDe) \approx 5$. For further details on the validation of the wave analysis and further information about the armour damage analysis, the reader is referred to Mares-Nasarre et al. (2022).

2.2. Selection of (dimensionless) variables

A selection of variables to include in the probabilistic framework is made, incorporating both the environmental conditions and properties related to the structure. The objective is to construct a model that is as simple as possible whilst accounting for the most relevant variables. The considered variables are defined as:

- Dimensionless armour damage at a given time, S_e (-), defined in Eq. (1). S_e has been reported to influence the increment of damage that the structure experiences due to a subsequent storm in studies such as Castillo et al. (2012) or Lira-Loarca et al. (2020).

- Increment of armour damage, ΔS_e (-), defined as the difference of S_e between subsequent measurements, here representing the effect of 1000 waves of a wave storm characterized by H_{m0} and T_p.
- Dimensionless water depth, h_s/H_{m0} (-). This random variable has been reported as significant to quantify armour damage in depth-limited conditions in studies such as Mares-Nasarre et al. (2022). This ratio has also been used to indicate whether waves are depth-limited (Nørgaard et al., 2014).
- Dimensionless wave steepness, $s_{0p} = H_{m0}/L_{0p}$ (-). The steepness influences the type of wave breaking on the structure slope and can be found in different studies and empirical formulas to compute armour damage (e.g. van der Meer, 1988; van Gent et al., 2003; Sande et al., 2018).
- Stability number, $N_s = H_{m0}/(\Delta D_n)$ (-), introduced by Hudson (1959), where $\Delta = (\rho - \rho_w)/\rho_w$ is the relative submerged mass density of armour units, being ρ the mass density of the armour units and ρ_w the mass density of the sea water. The stability number is one of the most common descriptors of hydraulic stability of the armour layer (e.g. Herrera et al., 2017; Mares-Nasarre et al., 2021; Yuksel et al., 2025). This variable includes the resistance of the armour elements to be displaced (Castillo et al., 2012).

The following experimental ranges of these variables were recorded: dimensionless water depth at the toe of the structure, $1.66 \leq h_s/H_{m0} \leq 7.36$; dimensionless wave steepness, $0.016 \leq H_{m0}/L_{0p} \leq 0.046$; stability number, $1.08 \leq N_s \leq 3.64$; dimensionless armour damage, $0.00 \leq S_e \leq 9.31$; and increment of dimensionless armour damage, $-0.11 \leq \Delta S_e \leq 2.61$. It should be noted that other relevant variables for hydraulic stability are not included due to experimental constrains. For instance, oblique wave attack with large incident angles significantly reduces the loading on the structure (Galland, 1994), more gentle armour slopes lead to more stable structures (Jumelet et al., 2024) or the presence of a berm in the front slope reduces the loading in the upper part of the slope (Yuksel et al., 2020).

3. Methodology

The following methodology is proposed to model armour damage progression in mound breakwaters:

1. Univariate parametric distributions are used to model the selected random variables, both related to the environmental conditions and resistance of the breakwater (see Section 2.2). The use of parametric distributions allows to infer values outside of the experimental ranges of the laboratory data.
2. The dependence between the considered random variables (see Section 2.2) is modelled using a Gaussian copula-based Bayesian Network (GCBN).
3. The GCBN is conditionalized using real wave data from a location of choice and a given D_n to generate synthetic damage curves.
4. The previously generated stochastic damage curves are used to quantify a gamma process, which models the survivability of the mound breakwater.

Fig. 3 shows these steps visually in a flow-chart. In the following sections, the different steps that comprise the proposed methodology are explained in further detail.

3.1. Bivariate copulas

Bivariate copulas are joint probability distribution functions that model the dependence between random variables with uniform margins. Sklar (1959) proposed a theorem according to which any multivariate joint distribution can be described in terms of univariate marginal distributions and a copula:

$$H_{X,Y}(x,y) = C\{F_X(x), G_Y(y)\} \tag{2}$$

where $H_{X,Y}(x,y)$ is the bivariate distribution with marginals $F_X(x)$ and $G_Y(y)$ in $[0,1]$ and $C\{F_X(x), G_Y(y)\}$ is the copula in the unit square $I^2 = ([0,1] \times [0,1])$ for all $(x,y) \in \mathbb{R}$.

Modelling joint distributions using copulas allows to independently model the distribution of the marginals and the dependence between them, providing more flexibility. A large variety of copula types is available in the literature (Genest and Favre, 2007). Fig. 4 displays 2000 samples of the most common copula types with Spearman rank correlation coefficient $r = 0.8$. Some of these are symmetrical (e.g. Gaussian, Frank, Student-t), whilst others display asymmetry (e.g. Clayton, Gumbel, Joe). Tail dependence refers to higher correlations in one of the extremes and therefore asymmetry.

In this research, the Gaussian copula is assumed to model the dependence between the random variables, which is defined as:

$$C_{X,Y}(u,v) = \Phi_2(\Phi^{-1}(u), \Phi^{-1}(v)|\rho_p) \tag{3}$$

where $\Phi_2\{..., ...|\rho_p\}$ is the bi-variate cumulative distribution function (CDF) of the normal distribution with Pearson's correlation coefficient ρ_p. Φ^{-1} is the inverse standard normal distribution function.

Due to the Gaussian copula assumption, asymmetries in the dependence between the random variables may not be captured. This assumption will be validated following the procedure described in Section 3.2.2.

3.2. Gaussian copula-based Bayesian network (GCBN)

As previously mentioned, the dependence between random variables is modelled with a GCBN. This section introduces the theory behind such models and describes the instruments used to validate them.

3.2.1. Concept of Gaussian copula-based Bayesian networks

A GCBN is a graphical model composed of a Directed Acyclic Graph (DAG) that describes the relationship between the random variables. Within the DAG, each node corresponds to a single random variable and each directed edge encodes a probabilistic dependence between the variables. In a DAG, node i represents a random variable X_i and has parent nodes $Pa(i) = i_1, \ldots, i_{p(i)}$. Hence, the edges always have a specified direction, from one node to another node. A DAG needs to be acyclic, meaning that the nodes are connected in a way that they never form a closed loop. In this study, GCBNs as defined by Hanea et al. (2006, 2015) are used. Each node is quantified with a univariate marginal distribution, which may be empirical or parametric, while the dependencies are modelled using Gaussian copulas and quantified using (un)conditional rank correlations. The first parent is associated with the unconditional rank correlation while subsequent parents are conditioned on previous parents. In this study, parametric distribution functions are used to quantify the nodes (see Section 3.3)

Rank correlation describes the relationship between the ranks of two random variables and can be quantified with the Spearman rank correlation coefficient (Spearman, 1904), defined as:

$$r = \frac{Cov(R_x, R_y)}{\sigma_{R_x}\sigma_{R_y}} \tag{4}$$

where $Cov(R_x, R_y)$ is the covariance of the ranked variables R_x and R_y, and σ_{R_x} and σ_{R_y} are their standard deviations. The statistic r ranges from -1 to $+1$, with the magnitude reflecting the strength of the monotonic association and the sign, the direction of such association. When $r = +1$ the dependence is perfect positive monotonic and when $r = -1$ the dependence is perfect negative monotonic. r can capture any monotonic relationship and not only linear relationships, differently to Pearson's correlation coefficient.

Considering three variables X_1, X_2 and X_3, there are different ways in which they can be connected, which affects their dependence structure:

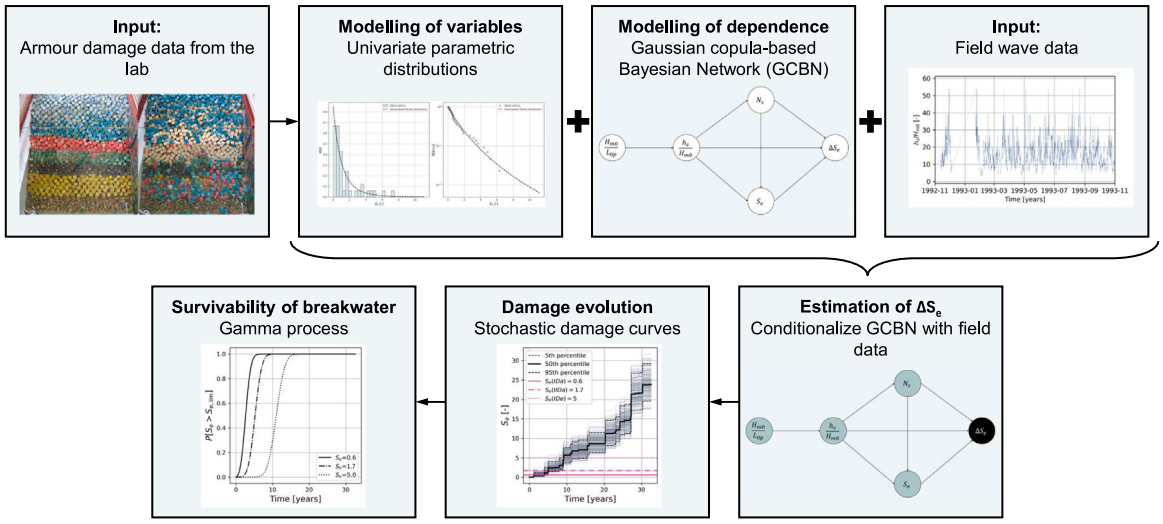

Fig. 3. Proposed methodology to model armour damage evolution of cube-armoured mound breakwaters.

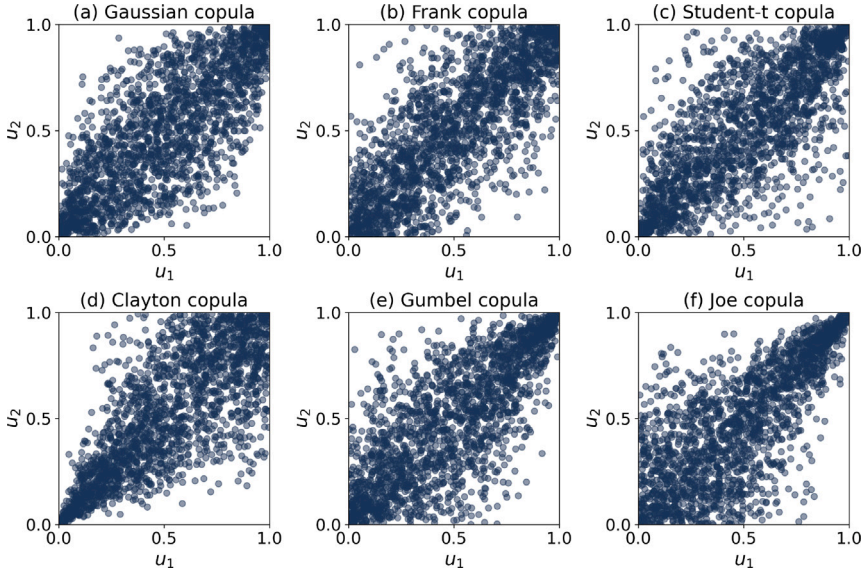

Fig. 4. 2000 samples of different copula types with $r = 0.8$: (a) Gaussian, (b) Frank, (c) Student-t (degrees of freedom $\nu = 4$), (d) Clayton, (e) Gumbel, and (f) Joe.

- $X_1 \rightarrow X_2 \rightarrow X_3$: X_1 influences X_2 and X_2 influences X_3. This implies that X_1 is dependent on X_3 ($X_1 \not\perp X_3$), but if the value of X_2 is given, they become independent ($X_1 \perp X_3 \mid X_2$).
- $X_1 \leftarrow X_2 \rightarrow X_3$: X_2 influences both X_1 and X_3. This means that X_1 and X_3 are conditionally independent given X_2 ($X_1 \perp X_3 \mid X_2$), but otherwise $X_1 \not\perp X_3$.
- $X_1 \rightarrow X_2 \leftarrow X_3$: X_1 and X_3 influence X_2 and therefore X_1 is independent of X_3 ($X_1 \perp X_3$). If X_2 is given, they however become dependent ($X_1 \not\perp X_3 \mid X_2$).

The dependence structure of a DAG can be described via a rank correlation matrix, following the protocol outlined by Hanea et al. (2006). This matrix, here referred to as R_{BN}, is composed of the unconditional rank correlations among the nodes. To implement the GCBN, the Python-based open-source toolbox PyBanshee is used (Koot et al., 2023).

3.2.2. Validation of Gaussian copula-based Bayesian networks

The validation of GCBNs has two objectives: (1) verify the Gaussian copula assumption, and (2) check whether the proposed DAG sufficiently captures the dependencies between variables.

Gaussian copulas are among the simplest types of copula, making GCBNs computationally efficient. However, they are unable to capture tail dependence and thus this assumption must be validated. One way to assess the Gaussian copula assumption is by fitting different copula families to each pair of variables, with and without tail dependence, and assessing the goodness of fit of those copulas to the data by computing the Cramér–von-Mises (CvM) metric (Berg, 2009) and Akaike Information Criterion (AIC) (Akaike, 1998). CvM metric measures the distance between the empirical and the parametric copula and is defined as:

$$S_{CvM} = n \sum_{i=1}^{n} ((C_n(u_i, v_i) - C_\theta(u_i, v_i))^2) \tag{5}$$

where $C_n(u_i, v_i)$ is the empirical copula, $C_\theta(u_i, v_i)$ is the parametric copula and n is the sample size. Hence, lower values of S_{CvM} indicate a better fit.

AIC is defined as:

$$AIC = 2k - 2\ln(\hat{L}) \tag{6}$$

where k is the number of estimated parameters in the model and $\hat{L}$ is the maximized value of the likelihood function for the model. The AIC introduces a penalty for the number of parameters, thereby favouring models with lower complexity.

In this study, Gaussian, Frank, Clayton and Gumbel copulas are fitted to each pair of variables using the available data and S_{CvM} and AIC are computed. Since Gaussian and Frank copulas are symmetric, they should yield the lowest values of both S_{CvM} and AIC if the data indeed does not present significant tail dependence.

To validate the proposed DAG, R_{BN} can be compared with both the empirical rank correlation matrix derived from the observations (R_E) and the matrix derived after transforming the data to standard normal space (R_N). Comparing R_{BN} and R_E assesses how well the defined DAG captures the dependencies present in the data. R_N represents a saturated DAG, where all nodes are interconnected, which represents the best possible model using GCBNs. However, a fully connected DAG lacks interpretability and may be an 'overfit' to the data (Mares-Nasarre, 2025), making it less attractive as a model. Comparing R_{BN} and R_N indicates how far the proposed DAG is from the best possible model. Furthermore, comparing R_E and R_N tests whether the Gaussian copula assumption adequately models the observed dependencies.

This comparison can be quantified by computing dissimilarity measures for Gaussian densities. Here, the *dependence calibration* or d-calibration score (d_c) based on the Hellinger distance defined in Morales-Nápoles et al. (2013a) is used. d_c is defined for the case of Gaussian copulas as:

$$d_c = 1 - d_H(N_1, N_2) = 1 - \sqrt{1 - \eta(N_1, N_2)} \tag{7a}$$

$$\eta(N_1, N_2) = \frac{|R_1|^{1/4}|R_2|^{1/4}}{\left|\frac{1}{2}R_1 + \frac{1}{2}R_2\right|^{1/2}} \tag{7b}$$

where $\eta(N_1, N_2)$ is the Hellinger distance, and R_1 and R_2 are the rank correlation matrices of the n-dimensional Gaussian copulas N_1 and N_2. A d_c closer to 1 indicates a smaller 'distance' between the two rank correlation matrices. According to studies such as (Mares-Nasarre, 2025) and Mendoza-Lugo et al. (2019), $d_c \geq 0.54$ are considered satisfactory.

For proofs regarding properties of d_c, the reader is referred to Rongen et al. (2025).

3.3. Univariate parametric distributions

Parametric distribution functions are used here to model each random variable in order to allow inference out of the experimental ranges. To this end, the following univariate marginal distributions are fitted to each random variable using the experimental data: normal, lognormal, exponential, gamma, beta, Rayleigh, uniform, generalized extreme value, gumbel, left-tailed gumbel, generalized pareto, student t, weibull, logistic, alpha, noncentral chi-squared and truncated normal distributions.

The selection of the most appropriate parametric distribution is based on AIC, the Kolmogorov–Smirnov (KS) test (Kolmogorov, 1933; Smirnov, 1949), and visual inspection of the probability density function (PDF) and cumulative distribution function (CDF) of the random variable.

The KS test is a formal hypothesis test that evaluates whether a sample comes from a specified parametric distribution by measuring the distance between the empirical distribution function of the sample and the CDF of the parametric distribution. The null hypothesis of this test states that the sample comes from the specified distribution. Thus, if the p-value exceeds the significance level, here 0.05, it is deemed reasonable to assume that the observations come from the specified parametric distribution.

In addition to quantitative measures, visual inspection of the PDF and CDF is conducted to assess the fit in the tails of the distribution, which may not be fully captured by the aforementioned statistics.

In summary, for each random variable, the distributions with a p-value for the KS-test above the chosen significance level of 0.05 are considered. Of these, the distributions with the lowest AIC and higher p-value of the KS-test are selected and analysed visually to check the behaviour in the tails.

3.4. Gamma process

A gamma process is a stochastic continuous-time process with independent, non-negative increments which follow a gamma distribution. They are useful to model systems in which measurements increase in small increments monotonically over time and are, therefore, applicable in condition- or time-based maintenance planning and optimization (van Noortwijk, 2009). The PDF of a random variable X that follows gamma distribution is defined as:

$$Ga(x \mid v, u) = \frac{u^v}{\Gamma(v)} x^{v-1} exp\{-ux\} I_{0,\infty}(x) \tag{8}$$

where $\Gamma(a) = \int_{z=0}^{\infty} z^{a-1}e^{-z}dz$ is the gamma function for $a > 0$; $I_A(x) = 1$ for $x \in A$ and $I_A(x) = 0$ for $x \notin A$. A gamma process $\{X(t), t \geq 0\}$ has the following properties:

1. $X(0) = 0$ with probability one;
2. $X(\tau) - X(t) \sim Ga(\cdot|v(\tau) - v(t), u)$ for all $\tau > t \geq 0$;
3. $X(t)$ has independent increments.

$v(t) > 0$ is a non-decreasing, right-continuous, real valued shape function with $v(0) \equiv 0$ for $t \geq 0$; and $u > 0$ is the scale parameter. To model the survivability of the breakwater, the CDF of the time to failure is necessary. A system fails when the stress s is greater than the resistance $R(t) = r_0 - X(t)$, where r_0 is the initial resistance. Let y be the damage level corresponding to failure, being defined as $y = r_0 - s$. In that case, the lifetime distribution of the time to failure can be defined as:

$$F(t) = Pr\{X(t) \geq y\} = \int_{x=y}^{\infty} f_{X(t)}(x)dx = \frac{\Gamma(v(t), yu)}{\Gamma(v(t))} \tag{9}$$

To quantify the gamma process, the Method of Moments is applied in this study. It is assumed that the expected value of the deterioration at time t is proportional to a power law, obtaining the following expressions for the first and second moments:

$$\mathbb{E}(X(t)) = \frac{v(t)}{u} = \frac{ct^b}{u}, \mathrm{Var}(X(t)) = \frac{v(t)}{u^2} = \frac{ct^b}{u^2} \tag{10}$$

where $b > 0$, $c > 0$ and $u > 0$. The most simple case is when the deterioration is linear in time and $b = 1$. This is called a stationary gamma process. If there is dependency between damage and the increment of damage at the next time step, it cannot be assumed that the gamma process is stationary and $b \neq 1$. Some examples of non-stationary gamma processes with the corresponding b in literature are creep ($b = 0.125$; Cinlar et al., 1977), scour-hole depth ($b = 0.4$; van Noortwijk and Klatter, 1999), diffusion-controlled ageing ($b = 0.5$; Ellingwood and Mori, 1993) and sulphate attack ($b = 2$; Ellingwood and Mori, 1993).

Since neither b, c or u are known, the Method of Moments is applied based on the simulated damage curves. For each time step t, the mean $\mu(t)$ and variance $\sigma^2(t)$ of S_e is computed. Using the expressions in Eq. (10), Method of Moments estimators are derived as $u_t = \mu(t)/\sigma^2(t)$ and $c_t = \mu(t)^2/(\sigma^2(t)t^b)$. Global estimates of u and c are obtained by averaging over time. To select the most appropriate value of the exponent b, a grid search is conducted over candidate values; $b = 0.8 - 3$ in steps of 0.1 are considered. For each tested b, the corresponding parameters u and c are estimated and the fitted mean and variance curves are compared with the empirical moments using the mean squared error. The value of b minimizing this error is selected as the best-fitting exponent together with the corresponding c and u to consequently calculate the probability that certain damage levels are exceeded in a particular time period.

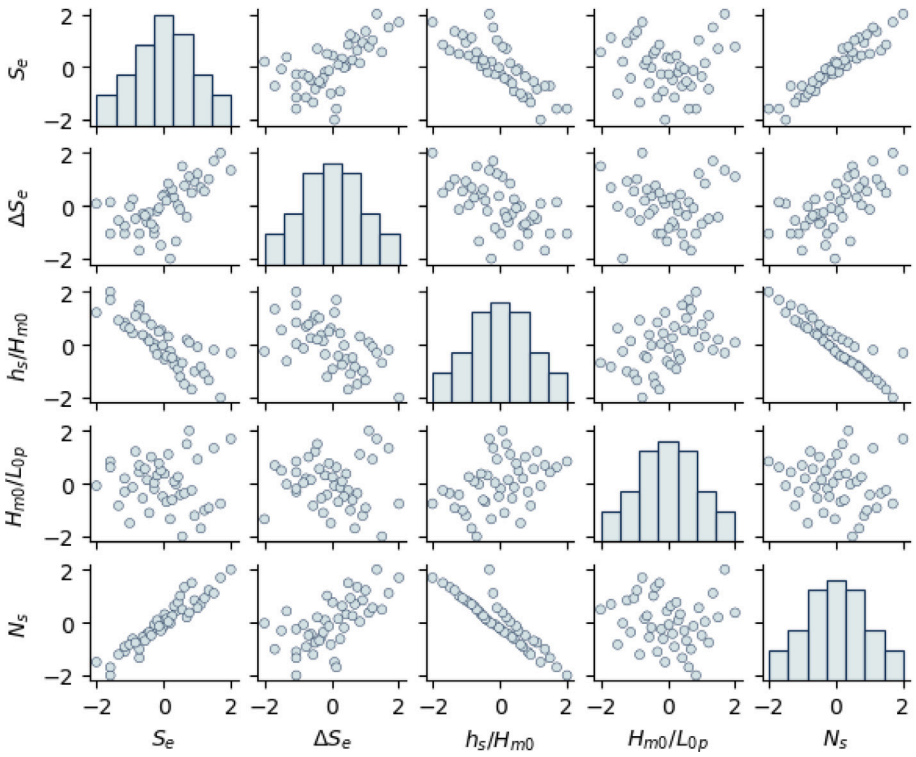

Fig. 5. Experimental data transformed to standard normal space: (diagonals) histograms, and (off diagonals) scatter plots, where S_e is the dimensionless damage parameter, ΔS_e is the increment of S_e between two successive storms, h_s/H_{m0} is the dimensionless water depth at the toe, H_{m0}/L_{0p} is the deep water wave steepness, and N_s is the stability number.

4. Construction and validation of the model

In this section, the probabilistic model is constructed and validated. To this end, the multivariate dependence between variables is modelled with a GCBN and the resulting model is validated using the criteria described in Section 3.2.2.

The construction of the model is based on the experimental data described in Section 2. Only the test series that reach a significant damage level are used for further analysis: h_s(m) = 0.3 with s_{0p} = 0.02 reaches S_e = 8.89, h_s(m) = 0.3 with s_{0p} = 0.03 reaches S_e = 4.28, and h_s(m) = 0.4 with s_{0p} = 0.05 reaches S_e = 9.31. In the other three test series, h_s(m) = 0.2 with s_{0p} = 0.02, h_s(m) = 0.2 with s_{0p} = 0.05, and h_s(m) = 0.3 with s_{0p} = 0.05, only a minimal damage level is reached (S_e = 0.97, 0.79 and 2.09 respectively) that can be attributed to the settlement of the armour units. Since the objective is to model long-term damage evolution, these become less relevant. This leads to a total of 44 experiments for further analysis.

4.1. Probabilistic analysis of experimental data

This section explores the probabilistic association between the selected variables in Section 2.2 in light of their physical relationships. Scatter plots of the random variables in standard normal space are displayed in Fig. 5.

Based on previous studies (Martín-Hidalgo et al., 2014; Marzeddu et al., 2020), a positive correlation between S_e and ΔS_e is expected. In other words, when the armour layer is already eroded, particularly when the filters become visible, the damage is expected to increase more rapidly due to the reduced resistance of the underlying materials. As shown in Fig. 5, the results indicate a positive dependence with upper tail dependence. This implies that the association between large values of ΔS_e and S_e is stronger than between low values of these variables. This means than once the structure presents a significant level of damage, deterioration occurs much faster.

A positive correlation is expected between S_e and N_s, and ΔS_e and N_s. N_s represents the ratio between the loading, H_{m0}, and the resistance, ΔD_n. Thus, the higher N_s, the greater the loading on the structure and, consequently, the greater the expected damage. As shown in Fig. 5, a positive dependence with some degree of upper tail dependence is observed. This indicates that deterioration tends to accelerate as the damage level in the structure increases, with stronger association occurring at higher values of the variables.

S_e and h_s/H_{m0}, and ΔS_e and h_s/H_{m0} are negatively correlated as, in general, higher H_{m0} leads to more damage. Finally, H_{m0}/L_{0p} presents a weak correlation with S_e and ΔS_e, although it is quite correlated with h_s/H_{m0}.

4.2. Construction of the model

First, the univariate parametric distributions are chosen for each random variable in the GCBN. Table 1 shows the chosen distributions and fitted parameters. More information about the parametric distributions can be found in Appendix A.

In order to define the DAG, the Spearman rank correlations, r, and associated p-values are computed for all pairs of variables. The empirical rank correlation matrix, including the p-values, collecting these results is displayed in Appendix B. Pairs with a significant r ($p - value < 0.05$) are connected in the DAG. Only the pairs S_e vs H_{m0}/L_{0p}, ΔS_e vs H_{m0}/L_{0p} and N_s vs H_{m0}/L_{0p} do not present a significant correlation. Arcs are added one by one from the largest to the smallest $|r|$ within those r found significant. After adding each arc, $d_c(R_{BN}, R_N)$ is computed and the arc is adopted if it results in an improvement $\Delta d_c(R_{BN}, R_N) \geq 0.01$. The process is stopped when there are no arcs left to add that lead to an improvement of $d_c(R_{BN}, R_N)$. The resulting DAG is shown in Fig. 6.

Table 1
Univariate marginal distribution of each random variable with its parameters.

Random variable	Parametric distribution	Parameters
Armour damage, S_e (–)	Generalized Pareto	$\xi = 0.23,\ \mu = 0,\ \sigma = 1.18$
Increment of armour damage ΔS_e (–)	Generalized Pareto	$\xi = 0.36,\ \mu = 0,\ \sigma = 0.42$
Dimensionless water depth, h_s/H_{m0} (–)	Lognormal	$\mu = 0.96,\ \sigma^2 = 0.21$
Dimensionless wave steepness, H_{m0}/L_{0p} (–)	Lognormal	$\mu = -3.66,\ \sigma^2 = 0.11$
Stability number, N_s (–)	Uniform	$a = 1.08,\ b = 3.64$

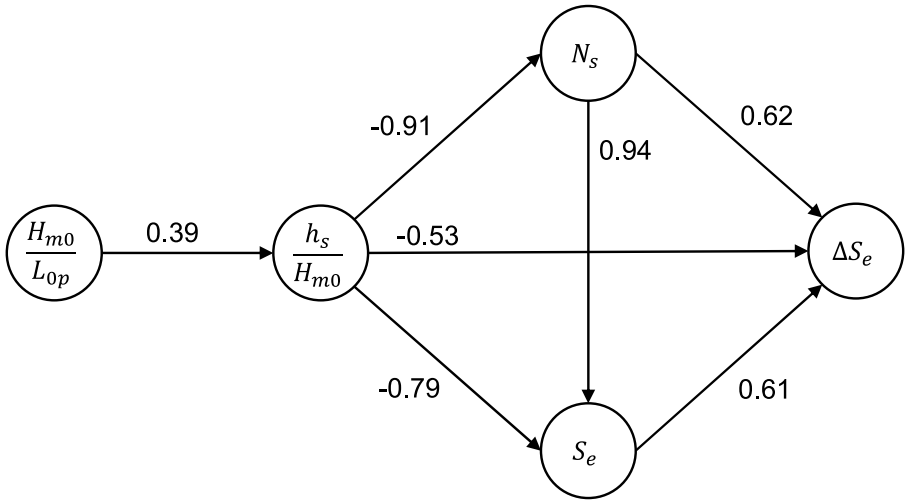

Fig. 6. Proposed DAG of the GCBN with the rank correlations in the arcs where H_{m0}/L_{0p} is the deep water wave steepness, h_s/H_{m0} is the dimensionless water depth at the toe, N_s is the stability number, S_e is the dimensionless damage parameter, and ΔS_e is the increment of S_e between two successive storms.

4.3. Validation of the model

As described in Section 3.2.2, the Gaussian copula assumption is verified by computing S_{CvM} and AIC for each pair between the observations and the fitted Clayton, Frank, Gaussian, and Gumbel copulas. Full results for S_{CvM} and AIC are shown in Appendix C. The Gaussian copula is selected as the best fit in 4 out of 10 pairs, and the Frank copula in another 4 pairs. However, in the other 2 pairs, an asymmetric copula (Gumbel) is selected as the best fit (S_e vs ΔS_e and ΔS_e vs h_s/H_{m0}). These two pairs display some degree of tail dependence which is not well represented by a symmetric copula. Regarding the AIC, either Gaussian or Frank perform the best in 7 out of 10 pairs (except in S_e vs ΔS_e, S_e vs H_{m0}/L_{0p}, and ΔS_e vs N_s). Overall, since in the majority of pairs (8 out of 10), a symmetric copula with no tail dependence is a satisfactory model, the Gaussian copula assumption is considered sufficient.

Furthermore, the rank correlation matrices displayed in Fig. 7 can be compared as explained in Section 3.2.2. In general, the same patterns are visible in the three matrices. The d-calibration score is computed for each pair of matrices to determine the 'distance' between the matrices with the following results: $d_c(R_E, R_N) = 0.76$, $d_c(R_N, R_{BN}) = 0.71$, and $d_c(R_E, R_{BN}) = 0.56$. This implies that the Gaussian copula assumption is reasonable for the tested data ($d_c(R_E, R_N) = 0.76$), the proposed DAG is close to the best possible model ($d_c(R_N, R_{BN}) = 0.71$), and the DAG captures the majority of dependencies present in the data ($d_c(R_E, R_{BN}) = 0.56$). Further information about the results of the d_c score is provided in Appendix D.

5. Example of application

Once the GCBN is constructed and validated, it is conditionalized with wave data from a chosen case study location to generate synthetic damage curves and quantify a gamma process. This allows to make the step from laboratory data to damage evolution estimations in real conditions. Here, an example is given for an idealized breakwater close to the port of Tarragona (Spain). Tarragona is located on the Costa Dorada at the Mediterranean Sea. The wave datasets are obtained from Puertos del Estado (Puertos del Estado, 2024), the authority responsible for Spanish state-owned ports. Data from buoy 1712 (41.07° N, 1.19° E) is used, which is part of the REDCOS dataset, which includes coastal buoys of Puertos del Estado. These buoys are located near port facilities and anchored at less than 100 m deep (Puertos del Estado, 2024). T_p and H_{m0} are available at an hourly rate in the time period between November 12, 1992 and June 11, 2025. No data is available for 0.89% of the measurements in the data series due to sensor failures or data transmission errors.

In order to calculate h_s/H_{m0}, H_{m0}/L_{0p} and N_s, it is assumed that $h_s = 13$ m, $\rho = 2300$ kg/m^3, $\rho_w = 1025$ kg/m^3, and $D_n = 2$ m. The following dimensionless ranges are obtained: $3.20 \leq h_s/H_{m0} \leq 108.33$, $0.00012 \leq H_{m0}/L_{0p} \leq 0.11$, and $0.05 \leq N_s \leq 1.63$.

The mean wave period T_m in the dataset ranges between 1.80 s and 10.51 s with 70% of the observations lying between 3.16 s and 4.95 s. Therefore, if outliers are ignored, the expected number of waves in one hour in the 70% confidence interval would be between 727.27 and 1139.24. That is approximately the same as the 1000 waves that are simulated in the laboratory test series. Therefore, the laboratory wave storms characterized by H_{m0} and T_p are interpreted as equivalent to a one-hour sea state from the field data with the same defining parameters.

Assuming an initial damage level at the beginning of measurements (November 12, 1992) of zero, $S_e = 0$, and using the values of h_s/H_{m0}, H_{m0}/L_{0p} and N_s computed for the first hour of field data, the GCBN is conditionalized to estimate the increment of damage ΔS_e through inference. It should be noted that the GCBN is a probabilistic model and, thus, it estimates the distribution of ΔS_e given the value of the conditioning random variables, here h_s/H_{m0}, H_{m0}/L_{0p}, N_s, and S_e. Therefore, here a random sample from the conditional distribution of ΔS_e is used. The obtained ΔS_e represents the increment of damage after the first hour. Then, ΔS_e is added to the previous existing damage level S_e (for the first time step, it is $S_e = 0$), and the process is repeated to

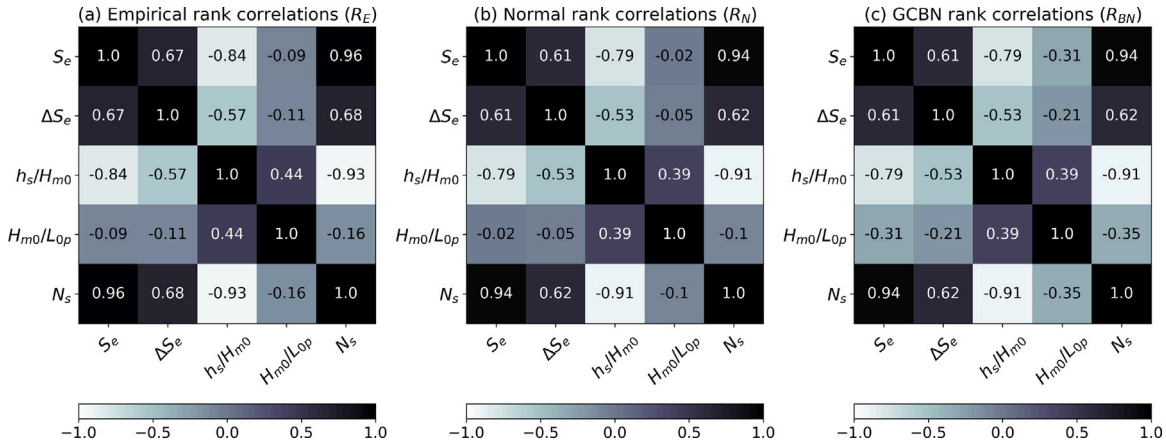

Fig. 7. Rank correlation matrices: (a) empirical rank correlations (R_E), (b) normal rank correlations (R_N), and (c) rank correlations of the proposed GCBN (R_{BN}). S_e is the dimensionless damage parameter, ΔS_e is the increment of S_e between two successive storms, h_s/H_{m0} is the dimensionless water depth at the toe, H_{m0}/L_{0p} is the deep water wave steepness, and N_s is the stability number.

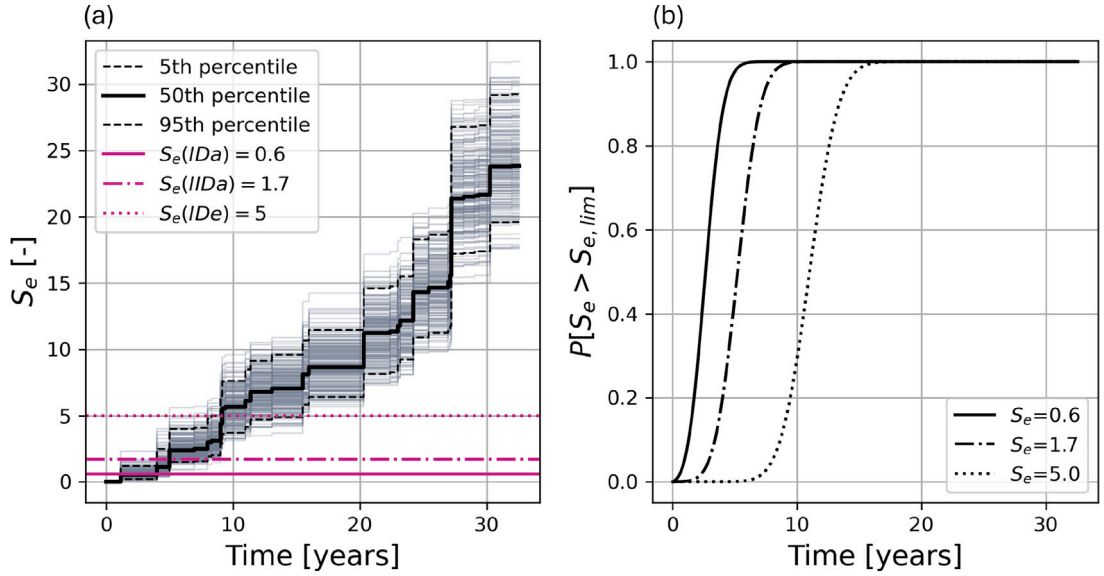

Fig. 8. Long-term damage progression of a hypothetical breakwater: (a) 200 synthetic damage curves, and (b) gamma process to model the survivability of the structure. S_e is the dimensionless damage parameter.

generate damage progression curves over the approximately 33 years of wave data. Following this process, a total of 200 synthetic damage progression curves (see Fig. 8(a)) are generated. From the laboratory data, it is observed that when $h_s/H_{m0} > 7.36$ and $N_s < 1.078$ no damage is generated, as it corresponds to very small wave heights. Hence, in these cases, a damage increment of zero is assigned. Fig. 8(a) also presents the 5th, 50th and 95th percentiles of the 200 generated damage curves, showing that uncertainty increases over time: the 90% confidence interval (difference between the 5th and 95th percentiles) becomes progressively wider as the damage level grows.

The synthetic damage curves are finally used to quantify a gamma process. Since there is a dependency between S_e and ΔS_e ($r = 0.67$), it is not reasonable to assume a stationary gamma process with $b = 1$. Instead, as described in Section 3.4, different values of b are tested ($b = 0.8 - 3$ in steps of 0.1) and, for each b, c and u are fitted using the Method of Moments. The combination with the lowest mean squared error is selected: $b = 1.4$, $c = 0.61$, and $u = 3.46$. In Fig. 8(b), the results of the gamma process are plotted for three damage levels corresponding to the initiation of damage ($S_e(IDa) = 0.6$), initiation of Iribarren damage ($S_e(IIDa) = 1.7$) and initiation of destruction ($S_e(IDe) = 5$), as defined by Mares-Nasarre et al. (2022). The plot can be used to determine the probability that certain damage levels are exceeded within a specified time period. For example, after 10 years the probability that the initiation of destruction is reached is 0.29. The goodness-of-fit of the gamma process is assessed in Appendix E by computing the coefficient of determination for the mean and variance.

6. Discussion and conclusion

This paper presents a probabilistic framework that combines a Gaussian copula-based Bayesian network with a gamma process to generate synthetic damage curves and quantify the evolution of long-term damage in mound breakwaters. In this paper, the application of the model is shown with a case study of an idealized breakwater close to the port of Tarragona. The GCBN is constructed from experimental data of non-overtopped cube-armoured breakwaters with an armour slope of $\cot\alpha = 3/2$ located in the depth-induced wave breaking zone (Mares-Nasarre et al., 2022) and includes as significant variables S_e, ΔS_e, h_s/H_{m0}, H_{m0}/L_{0p} and N_s. There are two main assumptions to validate when using a GCBN: (1) the use of the Gaussian copula to model the dependence between the pairs of variables, and (2) the defined DAG (see Fig. 6). The use of the Gaussian copula is first assessed using the

Cramér–von-Mises test; 80% of the variable pairs do not present significant tail dependence. Also, this assumption is validated by evaluating whether the proposed model sufficiently captures the dependencies in the data via the d-calibration score; $d_c(R_E, R_N) = 0.76$ indicates a satisfactory performance. Therefore, based on the available data, the use of Gaussian copulas to model the dependence between variables was considered reasonable. For applications in other conditions (e.g. other armour units, armour slopes, or overtopped structures), the GCBN must be revalidated with comparable experimental datasets (e.g. Mares-Nasarre et al., 2021; Gómez-Martín and Medina, 2014). In that case, the assumption of using a Gaussian copula to model the bivariate dependence between variables should be revisited. Gaussian copulas are symmetric and, thus, cannot account for asymmetries in the dependence structure. For instance, if a Gaussian copula was applied to model the dependence between S_e and ΔS_e in a dataset where strong upper tail dependence is observed in the data, the correlation between large values of S_e and ΔS_e would be underestimated leading to lower generated values of ΔS_e in the damage curves being thus in the unsafe side. Should the Gaussian copula prove inadequate, the GCBN could be replaced by a vine copula, which offers greater flexibility by allowing different types of copulas for each pair of variables (e.g. Paprotny et al., 2024).

In order to validate the constructed DAG, $d_c(R_N, R_{BN}) = 0.71$, and $d_c(R_E, R_{BN}) = 0.56$ are computed, indicating that the defined DAG reasonably approximates a saturated DAG (best possible model) and the data, respectively. Similarly, the dependence between pairs of variables would need to be reassessed and the DAG should be adjusted if necessary. Moreover, it should be noted that the experimental dataset used in this study did not include the influence of berms, and different armour layers and slopes. If the influence of such variables wants to be included in the methodology for design purposes, the GCBN can be modified to include them using an adequate experimental dataset or through expert elicitation (Rongen et al., 2025; Rongen and Morales-Nápoles, 2024).

A key strength of the proposed methodology is its adaptability to site-specific conditions. It can be applied using existing wave data, as demonstrated in this study, or using simulated wave data, for example, taking into account possible future scenarios, such as increased storm frequency or intensity due to climate change (e.g. Lucio et al., 2024). Consequently, the proposed framework is relevant both in the design phase of breakwaters to incorporate the performance along the design life of the structure, and support decision-making and cost estimations under different climate scenarios, and in later stages, for instance, for maintenance planning once the structure is operational. In this study, the application of the methodology was illustrated by calculating the exceedance probabilities for the three qualitative damage levels: initiation of damage ($S_e(IDa) = 0.6$), initiation of Iribarren damage ($S_e(IIDa) = 1.7$) and initiation of destruction ($S_e(IDe) = 5$). However, it should be noted that these definitions are case-specific (e.g. Herrera et al., 2017), and the methodology can be applied with any quantitative damage level. From the laboratory data, it was observed that when $h_s/H_{m0} > 7.36$ and $N_s < 1.078$ no damage was generated due to the limited wave heights. Therefore, when generating the synthetic damage curves $\Delta S_e = 0$ was assigned for the simulations with $h_s/H_{m0} > 7.36$ and $N_s < 1.078$. This assumption should also be revisited when using a different experimental dataset to apply the proposed methodology. Moreover, here, 200 synthetic curves were generated and used to quantify the gamma process. Actual applications of the proposed methodology may include a convergence test to determine the optimal number of simulations to quantify the parameters of the gamma process.

The literature on long-term damage evolution in mound breakwaters is scarce, limiting the possibilities for direct validation of the case study results against field data or studies in literature. Within the existing studies, Lira-Loarca et al. (2020) simulated storm events using statistical techniques for its application in the damage evolution of maritime structures. The authors exemplified the methodology with an idealized rock-armoured breakwater with $D_{n50} = 1.16$ m and armour slope $\cot\alpha = 2$ at the coast of Motril (Granada, Spain), whose cumulative damage was estimated using the empirical equation proposed in Melby and Kobayashi (1999). Lira-Loarca et al. (2020) estimated that the probability of an admissible failure (defined as $S_e = 6$ in Lira-Loarca et al., 2020) within the first seven years was 0.6. In this research, the probability of observing $S_e > 6$ after the first 7 years is 0.0018. The differences between those two values can be explained by a series of factors, which include: (1) the differences in the armour element of the two cases of study, (2) the differences in the method to compute damage, and (3) the differences in the wave climate. First, Lira-Loarca et al. (2020) used a rock-armoured mound breakwater with $D_{n50} = 1.16$ m in contrast with the case study used here which employs a cube-armoured mound breakwater with $D_n = 2$ m. As highlighted in previous literature (USACE, 1984; Mares-Nasarre et al., 2022), double-layer randomly-placed cube armours are more stable than double-layer randomly-placed rock-armours. For instance, USACE (1984) recommended the use of Hudson (1959)'s formula with stability coefficients $K_D = 6.5$ and 2.0 for double-layer randomly-placed cube armours and double-layer randomly-placed rock armours, respectively. Moreover, larger D_n leads to a higher weight of the elements in the armour and, thus, higher resistance of the armour layer to wave attack (e.g. van Gent et al., 2003; Mares-Nasarre et al., 2022). Second, Lira-Loarca et al. (2020) used Melby and Kobayashi (1999)'s formula to compute the damage. The experimental methodology used in Melby and Kobayashi (1999) to derive the damage formula presents relevant differences when compared with the experiments performed in Mares-Nasarre et al. (2022), such as the used wave spectrum and the length of the test series. Melby and Kobayashi (1999) used a TMA spectrum and measured damage after each 30 min, while Mares-Nasarre et al. (2022) used a JONSWAP spectrum ($\gamma = 3.3$) with test series of 1000 waves and, thus, variable test duration as function of the tested wave period. Finally, wave conditions are different as the locations of the case study are different; Lira-Loarca et al. (2020) locates the case study in the South of the Mediterranean sea (Motril, Spain), while the present study uses wave data from the North of the Mediterranean sea (Tarragona, Spain).

Nonetheless, considering the design life of most mound breakwaters (typically 50 years; Puertos del Estado, 2012), the current model produces conservative estimations of the damage evolution. This can partially be attributed to the exclusion of oblique wave attack from the analysis. Several studies have demonstrated that oblique waves result in significantly lower loadings in the structures compared to perpendicular wave attack, particularly at larger incidence angles (e.g. Galland, 1994; van Gent, 2014; Wolters and van Gent, 2011). This reduces the required armour size and results in lower damage levels. As an example, at the case study location, wave approach angles span nearly 90° (see Fig. 9). Hence, independently of the orientation of a breakwater, there will always be oblique wave attack to a certain extent. Most laboratory experiments, in contrast, are performed in wave flumes with perpendicular wave attack. Consequently, if damage data for oblique wave attack becomes available, the model could be recalibrated by adding wave angle incidence as a variable to the GCBN, thereby providing less conservative estimations of damage evolution.

The insights provided by the proposed methodology on the survivability of mound breakwaters can be useful to assess the behaviour of the structures along their life span during the design phase, as well as optimize maintenance inspections and scheduling (Golestani et al., 2023). For example, port authorities can determine tolerable damage levels for their breakwaters and use the probabilities that these levels are exceeded to determine the frequency of maintenance actions.

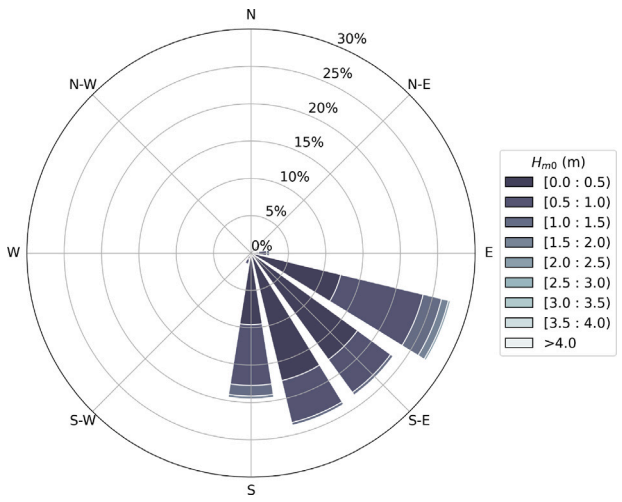

Fig. 9. Directional wave rose close to the port of Tarragona, where H_{m0} is the spectral significant wave height.

Notation

Acronyms

De	Qualitative damage level of Destruction (Losada et al., 1986; Vidal et al., 1991)
CDF	Cumulative distribution function
CvM	Cramér–von Mises
DAG	Directed Acyclic Graph
GCBN	Gaussian Copula-based Bayesian Networks (Hanea et al., 2006, 2015)
HeP	Heterogeneous Packing defined in Gómez-Martín and Medina (2014)
IDa	Qualitative damage level of Initiation of damage (Losada et al., 1986; Vidal et al., 1991)
IIDa	Qualitative damage level of Initiation of Iribarren damage (Losada et al., 1986; Vidal et al., 1991)
KS	Kolmogorov–Smirnov
PDF	Probability density function
UPV	*Universitat Politècnica de València*

Symbols

α (°)	Slope angle of the mound breakwater
γ (–)	Peak enhancement factor of JONSWAP spectrum
$\Gamma(a) = \int_{z=0}^{\infty} z^{a-1} e^{-z} dz$ (–)	Gamma function for $a > 0$; $I_A(x) = 1$ for $x \in A$ and $I_A(x) = 0$ for $x \notin A$
$\Delta = (\rho - \rho_w)/\rho_w$ (–)	Relative submerged mass density of the armour unit
ΔS_e (–)	Increment of S_e between two test runs
$\eta(N_1, N_2) = \frac{\lvert R_1\rvert^{1/4}\lvert R_2\rvert^{1/4}}{\left\lvert \frac{1}{2}R_1+\frac{1}{2}R_2\right\rvert^{1/2}}$ (–)	Hellinger distance for n-dimensional Gaussian copulas N_1 and N_2 computed between their rank correlation matrices R_1 and R_2
μ (–)	Location parameter of a parametric distribution function
$\mu(t)$ (–)	Mean of S_e at time t
ξ (–)	Shape parameter of a parametric distribution function
ρ (g/cm^3)	Mass density of the armour unit
ρ_p (–)	Pearson's correlation coefficient
ρ_w (g/cm^3)	Mass density of sea water
σ (–)	Scale parameter of a parametric distribution function
$\sigma^2(t)$(–)	Variance of S_e at time t
σ_{R_X}, σ_{R_Y} (–)	Standard deviation of the rank variables R_X and R_y, respectively
Φ^{-1} (–)	Inverse of the standard normal distribution function
Φ_2 (–)	Bivariate standard normal cumulative distribution function
Φ_p (–)	Packing density of the armour layer
a_u, b_u (–)	Parameters of uniform distribution function
A_e (cm^2)	Eroded area in the cross section
$AIC = 2k - 2ln(\hat{L})$	Akaike Information Criterion
b (–)	Power in $v(t)$
c (–)	Coefficient in $v(t)$
$C_\theta(u_i, v_i)$ (–)	Parametric bivariate copula
$C_n(u_i, v_i)$ (–)	Empirical bivariate copula
$c_t = \mu(t)^2/(\sigma^2(t)t^b)$ (–)	Moment estimator of c
$C_{X,Y}(u, v)$ (–)	Bivariate copula of random variables X and Y
$Cov(R_x, R_y)$ (–)	Covariance of the ranked variables R_x and R_y
$d_c = 1 - d_H(N_1, N_2) = 1 - \sqrt{1 - \eta(N_1, N_2)}$	d-calibration score computed between the n-dimensional Gaussian copulas N_1 and N_2 defined by Morales-Nápoles et al. (2013a)
$D_n = M/\rho$ (cm)	Nominal diameter of the armour unit
$D_{n50} = M/\rho$ (cm)	Nominal stone diameter
f_i (–)	Fitted/predicted values in coefficient of determination
$F_X(x)$ (–)	Marginal distribution of random variable X
g (m/s^2)	Gravitational acceleration
$G_Y(y)$ (–)	Marginal distribution of random variable Y
$Ga(x \mid v, u)$	PDF of the Gamma distribution function
H_0 (–)	Null hypothesis
H_a (–)	Alternative hypothesis
$H_{m0} = 4(m_0)^{0.5}$ (m)	Spectral significant wave height, where m_0 is zeroth-order spectral moment
h_s (m)	Water depth at the toe of the structure
$H_{X,Y}(x, y)$ (–)	Bivariate joint distribution of the random variables X and Y
k (–)	Number of estimated parameters in the model
K_D (–)	Stability coefficient in Hudson formula (Hudson, 1959)
$\hat{L}$ (–)	Maximized value of the likelihood function for the model
$L_{0p} = gT_p^2/2\pi$ (m)	Deep-water wave length computed with T_p
M (g)	Mass of the armour unit
n (–)	Sample size
$N_s = \frac{H_{m0}}{\Delta D_n}$ (–)	Stability number
$Pa(i)$ (–)	Parent nodes of random variable X_i
r (–)	Spearman's rank correlation coefficient
r_0 (–)	Initial resistance of the system
R^2 (–)	Coefficient of determination
$R(t) = r_0 - X(t)$ (–)	Resistance of the system
R_{BN} (–)	Rank correlation matrix derived from the GCBN following the protocol in Hanea et al. (2006, 2015)
R_E (–)	Empirical rank correlation matrix derived from observations
R_N (–)	Rank correlation matrix computed after transforming the data to standard normal space
s (–)	Stress of the system

$s_{0p} = H_{m0}/L_{0p}$ (–)	Wave steepness
$S_{CvM} = n\sum_{i=1}^{n}((C_n(u_i, v_i) - C_\theta(u_i, v_i))^2)$ (–)	Cramér–von-Mises statistic
$S_e = \frac{A_e}{D_{n50}^2}$ (–)	Dimensionless damage as defined by Broderick (1983)
S_i (–)	Damage in each strip following the Virtual Net method by Gómez-Martín and Medina (2006)
t (s)	Time instant
T_m (s)	Temporal mean wave period
T_p (s)	Peak wave period
u (–)	Scale parameter of the Gamma process
$u_t = \mu(t)/\sigma^2(t)$ (–)	Moment estimator for u
$v(t)$ (–)	Shape function of the Gamma process
$X(t)$ (–)	Damage of the system at time t
X_i (·)	Random variable i
y (–)	Damage level corresponding to failure
$\bar{y} = \frac{1}{n}\sum_{i=1}^{n} y_i$ (–)	Mean of observed data
y_i (–)	Values of the dataset used to compute the coefficient of determination

CRediT authorship contribution statement

P. Andrés-Wörz: Writing – original draft, Methodology, Conceptualization. **O. Morales-Nápoles:** Writing – review & editing, Conceptualization. **P. Mares-Nasarre:** Writing – review & editing, Data curation, Conceptualization.

Declaration of competing interest

The authors declare that they have no known competing financial interests or personal relationships that could have appeared to influence the work reported in this paper.

Acknowledgement

The authors would like to acknowledge Puertos del Estado for providing the wave dataset used in this study. The authors also acknowledge the experimental data used in this study that was retrieved through the grant BIA2012-33967 supported by the Spanish Ministry of Economy and Competitiveness.

Appendix A. Univariate parametric distributions

In this Appendix, information about the univariate parametric distributions chosen to model each variable will be provided. Each plot in this Appendix shows the probability density function on the left and the survival function on the right. The survival function is equivalent to $1 - F(x)$ where $F(x)$ is the cumulative distribution function. The survival function represents the probability that the random variable X is greater than x; $P[X > x]$.

The generalized pareto distribution (GPD) is described by the parameters $\xi \in (-\infty, \infty)$ (shape), $\mu \in (-\infty, \infty)$ (location) and $\sigma \in (0, \infty)$ (scale). The PDF of a variable X with a GPD ($X \sim GPD(\xi, \mu, \sigma)$) is:

$$f_{(\xi,\mu,\sigma)}(x) = \frac{1}{\sigma}(1 + \frac{\xi(x-\mu)}{\sigma})^{-(1+1/\xi)} \tag{A.1}$$

The CDF of $X \sim GPD(\xi, \mu, \sigma)$ is given by:

$$F_{(\xi,\mu,\sigma)}(x) = \begin{cases} 1 - (1 + \frac{\xi(x-\mu)}{\sigma})^{-1/\xi} & \text{for } \xi \neq 0 \\ 1 - \exp(-\frac{x-\mu}{\sigma}) & \text{for } \xi = 0 \end{cases} \tag{A.2}$$

where the support of X is dependent on the sign of ξ: $x \geq \mu$ when $\xi \geq 0$, and $\mu \leq x \leq \mu - \sigma/\xi$ when $\xi < 0$. Fig. A.1 shows the empirical and parametric distributions of $S_e \sim GPD(\xi = 0.23, \mu = 0, \sigma = 1.18)$ and Fig. A.2 of $\Delta S_e \sim GPD(\xi = 0.36, \mu = 0, \sigma = 0.42)$.

A variable X has a lognormal distribution if its natural logarithm has a normal distribution with mean μ and variance σ^2 ($\ln X \sim \mathcal{N}(\mu, \sigma^2)$). The PDF of $X \sim Lognormal(\mu, \sigma^2)$ is defined as:

$$f_{\mu,\sigma^2}(x) = \frac{1}{x\sigma\sqrt{2\pi}} \exp(-\frac{(\ln x - \mu)^2}{2\sigma^2}) \tag{A.3}$$

The CDF of the lognormal distribution $X \sim Lognormal(\mu, \sigma^2)$ is:

$$F_{\mu,\sigma^2}(x) = \Phi(\frac{\ln x - \mu}{\sigma}) \tag{A.4}$$

where Φ is the CDF of the standard normal distributions $\mathcal{N}(0, 1)$. Fig. A.3 shows the empirical and parametric distribution of $h_s/H_{m0} \sim Lognormal(\mu = 0.96, \sigma^2 = 0.21)$ and Fig. A.4 of $H_{m0}/L_{0p} \sim Lognormal(\mu = -3.66, \sigma^2 = 0.11)$.

The continuous uniform distribution is defined by the parameters a_u and b_u, where $-\infty < a_u < b_u < \infty$, and a_u and b_u are the minimum and maximum values respectively. The PDF of a random variable X with a uniform distribution ($X \sim U(a_u, b_u)$) is:

$$f_{(a_u,b_u)}(x) = \begin{cases} \frac{1}{b_u - a_u} & \text{for } a_u \leq x \leq b_u, \\ 0 & \text{for } x < a_u \text{ or } x > b_u. \end{cases} \tag{A.5}$$

The CDF of $X \sim U(a, b)$ is:

$$F_{(a_u,b_u)}(x) = \begin{cases} 0 & \text{for } x < a_u, \\ \frac{x - a_u}{b - a_u} & \text{for } a_u \leq x \leq b_u, \\ 1 & \text{for } x > b_u. \end{cases} \tag{A.6}$$

Fig. A.5 shows the empirical and parametric distribution of $N_s \sim U(a_u = 1.08, b_u = 3.64)$.

Appendix B. Empirical rank correlations and p-values

Fig. B.1 shows the empirical rank correlations observed in the laboratory data as well as the corresponding p-values. The null hypothesis (H_0) corresponds to no correlation existing between the variables, whilst the alternative hypothesis (H_a) states that there is correlation. Hence, considering a significance level of $\alpha = 0.05$, any $p - value < 0.05$ justifies rejecting H_0 and suggests that significant correlation exists.

Appendix C. Validation of the Gaussian copula assumption

Fig. C.1 shows the results of the Cramér–von-Mises statistic and Fig. C.2 the results of the AIC for the four tested copula types (Clayton, Frank, Gaussian and Gumbel) for all the pairs of variables.

Appendix D. D-calibration scores

To assess the significance of the d-calibration scores computed in Section 4.3, a hypothesis test as described in Morales-Nápoles et al. (2013b) or Mendoza-Lugo et al. (2019) is conducted. To this end, distributions are generated by repeatedly sampling multivariate normal data using either R_N or R_{BN} and computing the pairwise d_c scores. The observed scores computed in Section 4.3 are compared against the simulated distributions, giving an indication of the significance of the scores.

Fig. D.1(a) shows that $d_c(R_E, R_N)$ is within the 90% confidence interval of the normal distribution $d_c(R_N, R_N)$ when drawing 85 samples of the normal distribution and performing 500 iterations. This corroborates the assumption of using a Gaussian copula in the Bayesian network model. Fig. D.1(b) shows that $d_c(R_N, R_{BN})$ is within the 90% confidence interval of the distribution $d_c(R_{BN}, R_{BN})$ when drawing 60 samples and performing 500 iterations. This indicates that the DAG is satisfactory, given the assumption of using Gaussian copulas.

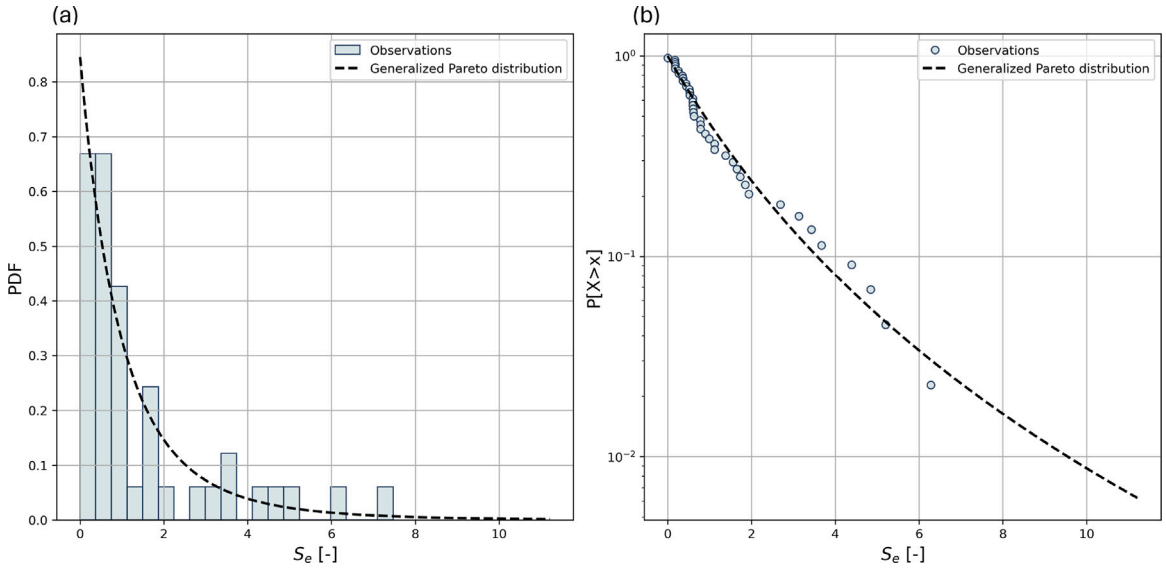

Fig. A.1. Empirical and parametric distribution of the dimensionless damage parameter, S_e: (a) probability density function, and (b) survival function.

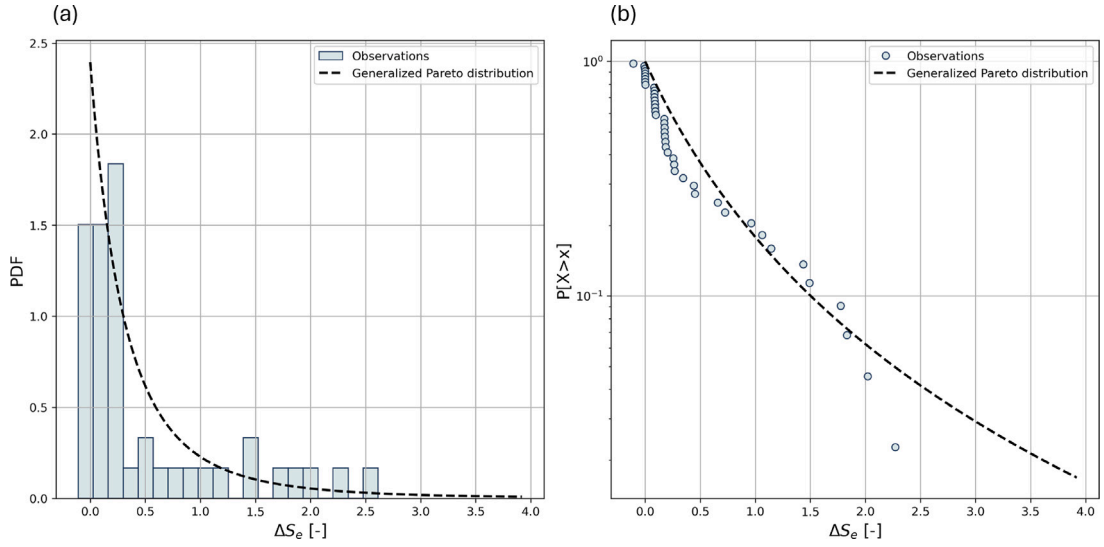

Fig. A.2. Empirical and parametric distribution of the increment of the dimensionless damage parameter between two consecutive wave storms, ΔS_e: (a) probability density function, and (b) survival function.

Appendix E. Goodness-of-fit of gamma process

The goodness-of-fit of the fitted gamma process ($b = 1.4$, $c = 0.61$ and $u = 3.46$) can be validated both visually and quantitatively. Fig. E.1(a) plots the target mean against the predicted mean from the fitted gamma process and Fig. E.1(b) does the same thing for the variance. If the gamma process is a good fit, points will lie close to the line $y = x$, which represents the ideal fit. The fit can also be assessed quantitatively by computing the coefficient of determination ($0 \leq R^2 \leq 1$) for the mean and variance, which is defined as:

$$R^2 = 1 - \frac{\sum_i (y_i - f_i)^2}{\sum_i (y_i - \bar{y})^2} \tag{E.1}$$

where y_i are the n values of the studied dataset, f_i are the associated fitted/predicted values, and $\bar{y} = \frac{1}{n}\sum_{i=1}^{n} y_i$ is the mean of the observed data. Values of R^2 closer to 1 indicate a better fit since the modelled and

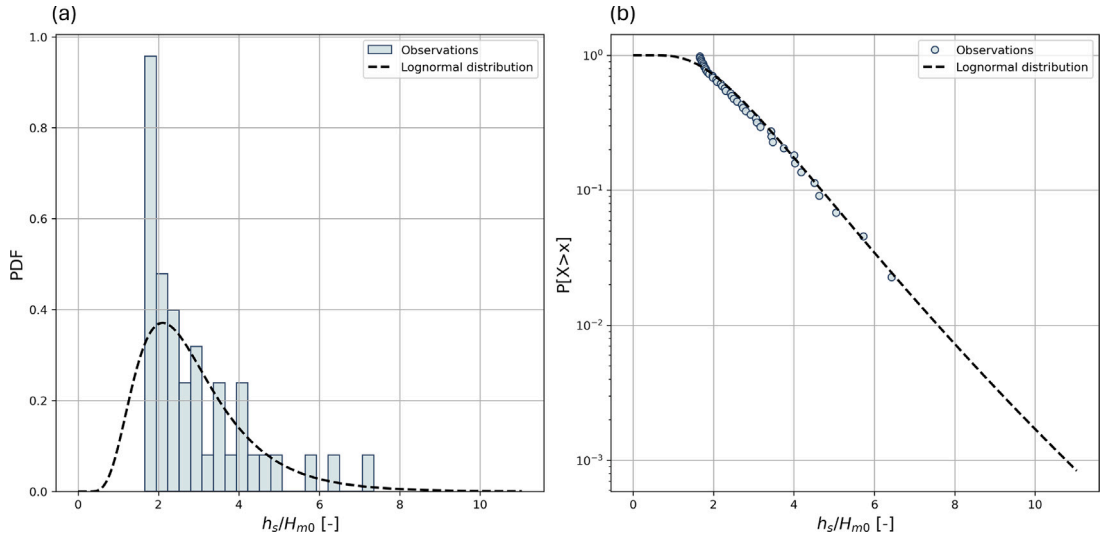

Fig. A.3. Empirical and parametric distribution of the dimensionless water depth, h_s/H_{m0}: (a) probability density function, and (b) survival function.

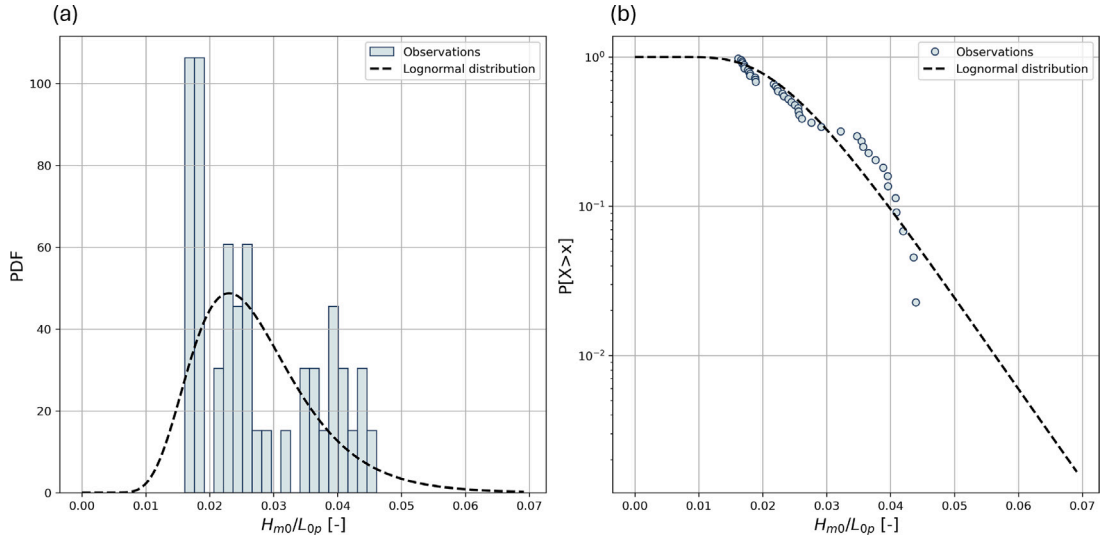

Fig. A.4. Empirical and parametric distribution of the deep wave steepness, H_{m0}/L_{0p}: (a) probability density function, and (b) survival function.

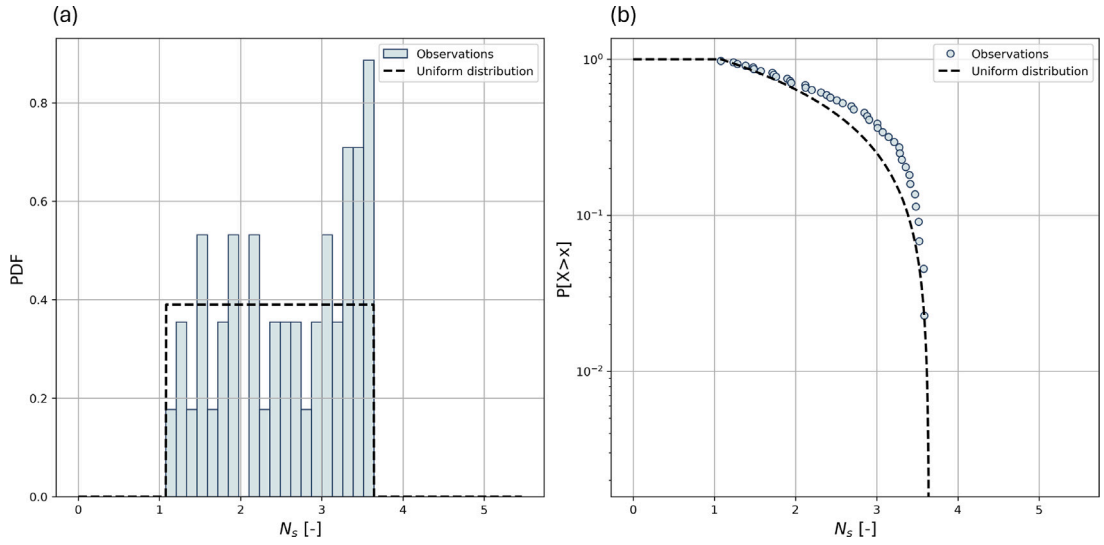

Fig. A.5. Empirical and parametric distribution of the stability number, N_s: (a) probability density function, and (b) survival function.

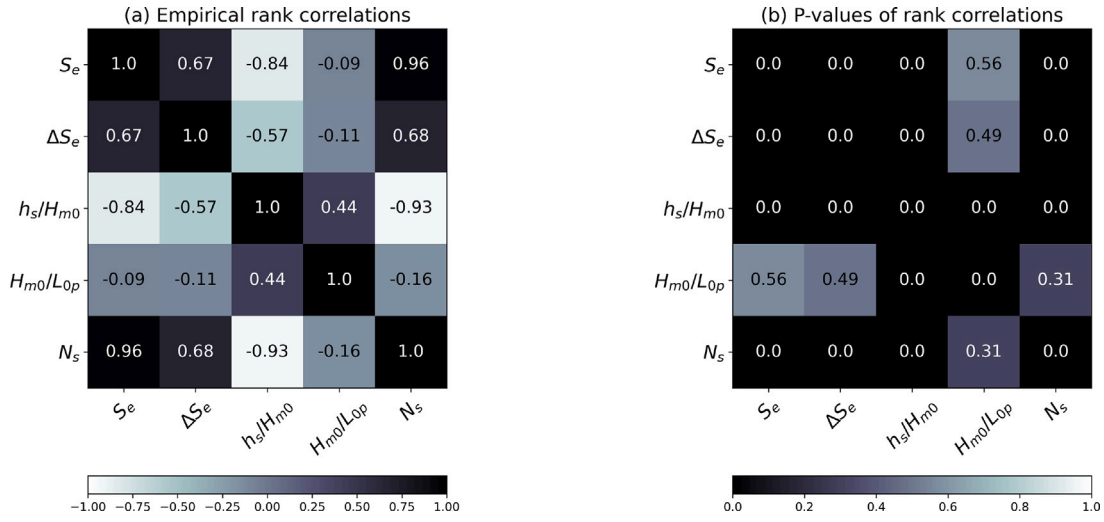

Fig. B.1. Empirical rank correlations: (a) Empirical rank correlation matrix (R_E), and (b) p-values of empirical rank correlations. S_e is the dimensionless damage parameter, ΔS_e is the increment of S_e between two successive storms, h_s/H_{m0} is the dimensionless water depth at the toe, H_{m0}/L_{0p} is the deep water wave steepness, and N_s is the stability number.

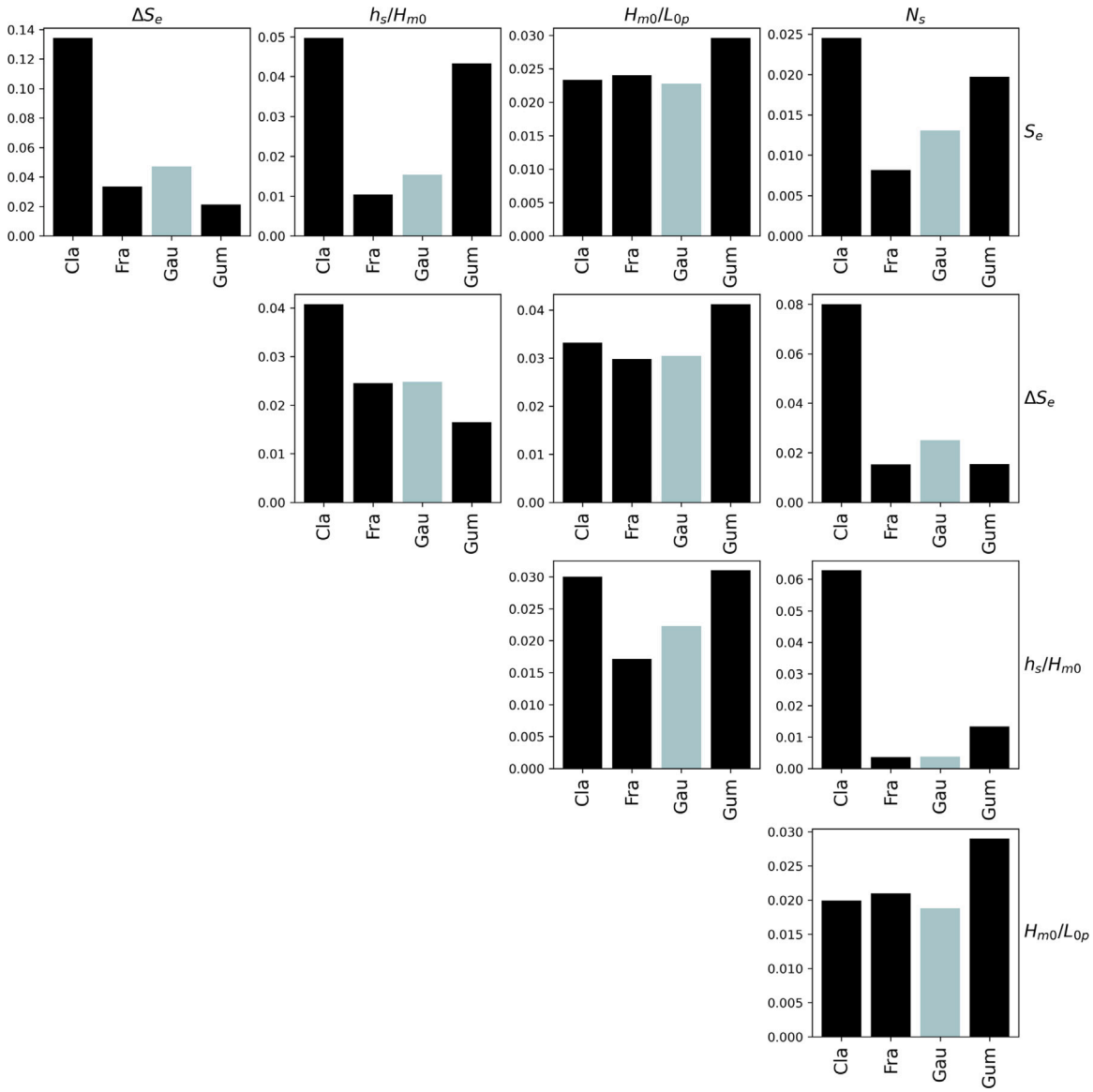

Fig. C.1. Comparison of results of the Cramér–von-Mises statistic of the Clayton, Frank, Gaussian and Gumbel copulas for all pairs of variables, where S_e is the dimensionless damage parameter, ΔS_e is the increment of S_e between two successive storms, h_s/H_{m0} is the dimensionless water depth at the toe, H_{m0}/L_{0p} is the deep water wave steepness, and N_s is the stability number.

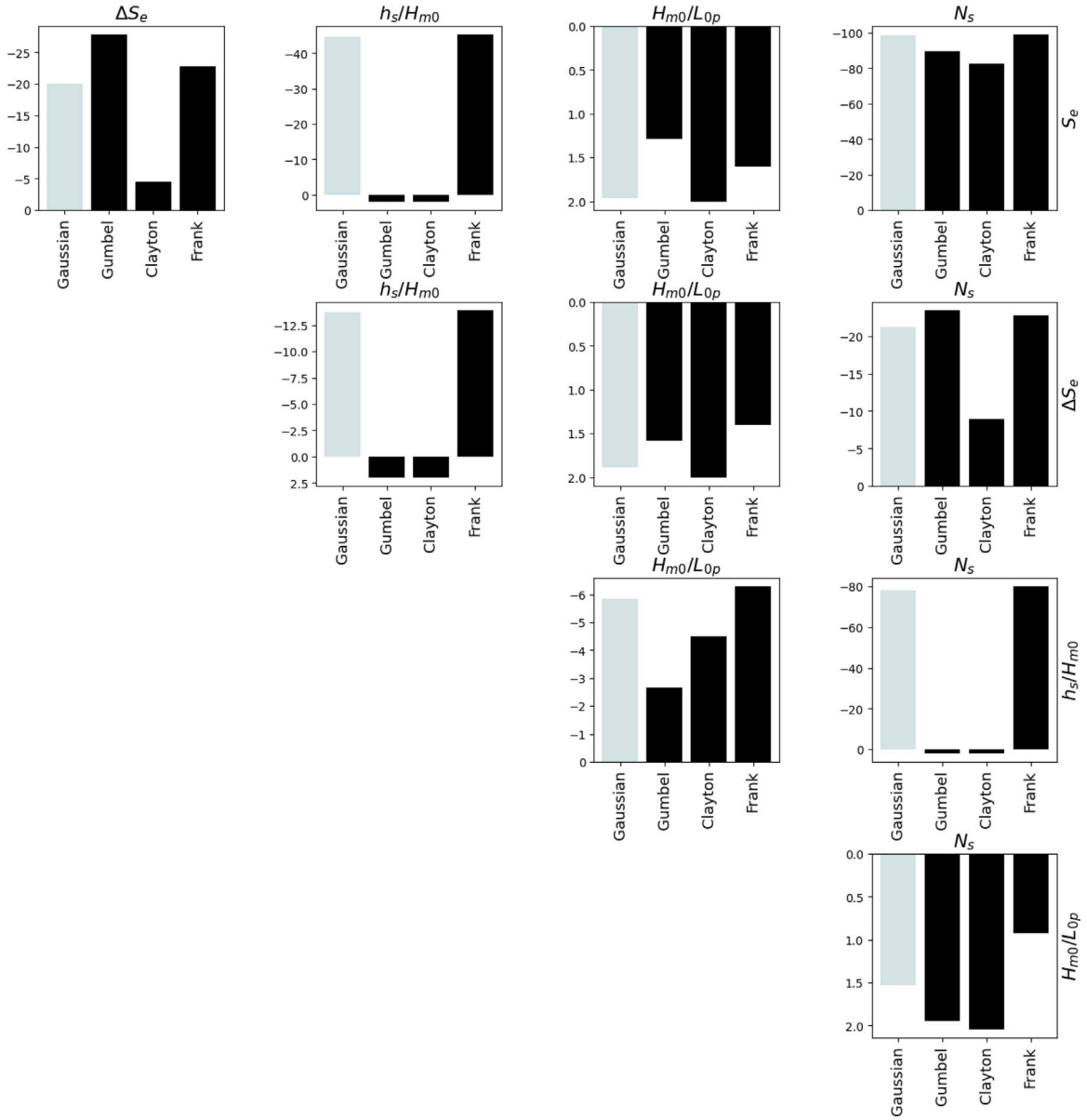

Fig. C.2. Comparison of results of Akaike Information Criterion, AIC, of the Clayton, Frank, Gaussian and Gumbel copulas for all pairs of variables, where S_e is the dimensionless damage parameter, ΔS_e is the increment of S_e between two successive storms, h_s/H_{m0} is the dimensionless water depth at the toe, H_{m0}/L_{0p} is the deep water wave steepness, and N_s is the stability number.

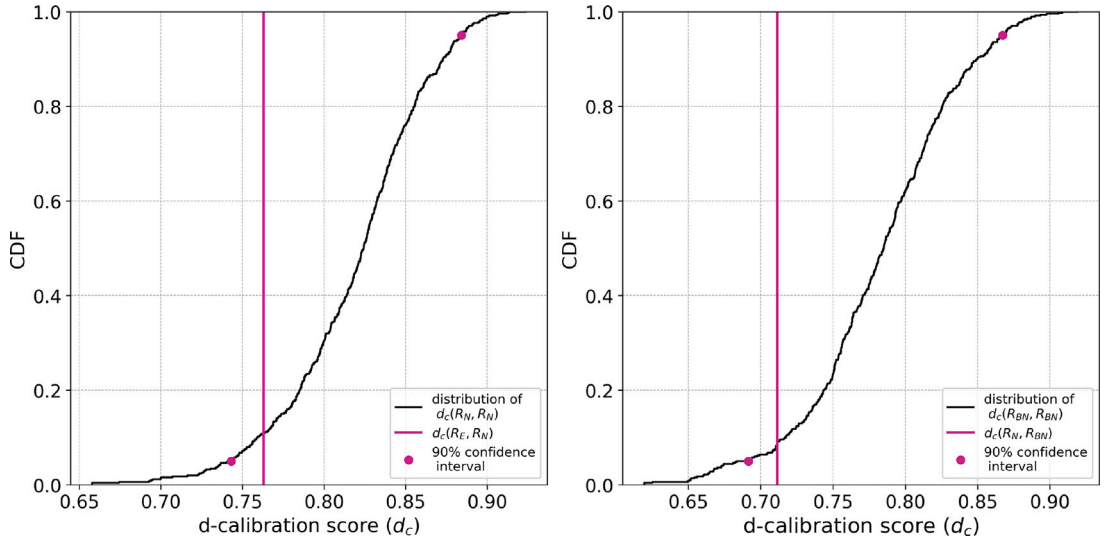

Fig. D.1. (a) $d_c(R_E, R_N)$ in the distribution of $d_c(R_N, R_N)$ with 85 samples in 500 iterations, and (b) $d_c(R_N, R_{BN})$ in the distribution of $d_c(R_{BN}, R_{BN})$ with 60 samples in 500 iterations.

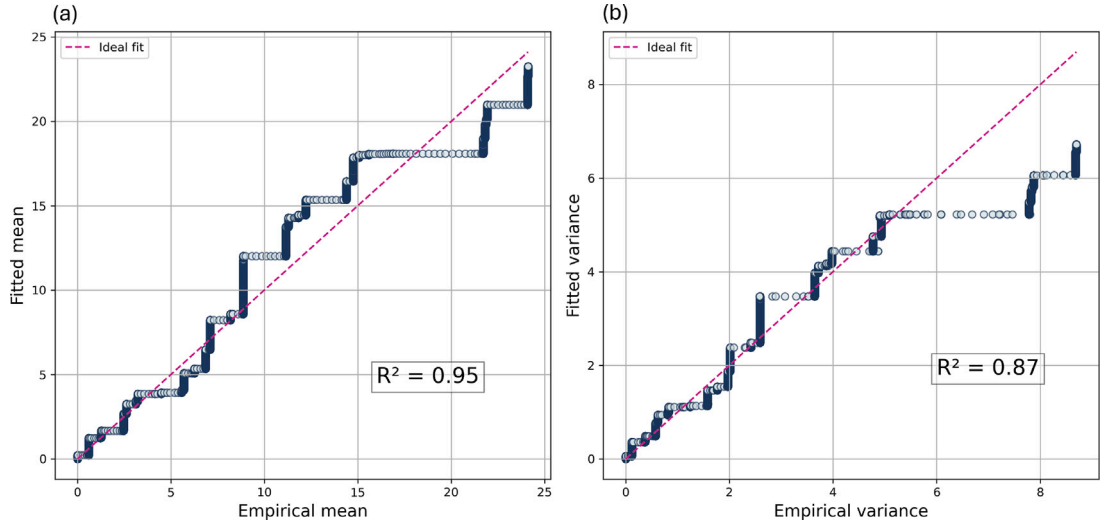

Fig. E.1. Goodness-of-fit of the gamma process with $b = 1.4$, $c = 0.61$ and $u = 3.46$ estimated with the Method of Moments: (a) Empirical mean vs fitted mean ($R^2 = 0.95$), and (b) Empirical variance vs fitted variance ($R^2 = 0.87$).

observed values are 'closer'. R^2 is computed separately for the mean and variance: $R^2 = 0.95$ for the mean and $R^2 = 0.87$ for the variance.

References

Akaike, H., 1998. Information theory and an extension of the maximum likelihood principle. In: Selected Papers of Hirotugu Akaike. Springer New York, pp. 199–213. http://dx.doi.org/10.1007/978-1-4612-1694-0_15.

Allsop, W., Cork, R., Verhagen, H., 2010. A database of major breakwaters around the world. Edinburgh, In: ICE Breakwaters Conference, vol. 2, URL: https://www.researchgate.net/publication/38144785_A_Database_of_Major_Breakwaters_Around_the_World.

Barros, B., Conde, B., Riveiro, B., Morales-Nápoles, O., 2024. Gaussian copula-based Bayesian network approach for characterizing spatial variability in aging steel bridges. Struct. Saf. 106, 102403. http://dx.doi.org/10.1016/j.strusafe.2023.102403.

Berg, D., 2009. Copula goodness-of-fit testing: an overview and power comparison. Eur. J. Financ. 15 (7–8), 675–701. http://dx.doi.org/10.1080/13518470802697428.

Broderick, L., 1983. Riprap stability. a progress report. In: Proc. Specialty Conference on Design, Construction, Maintenane and Performance of Coastal Structures, ASCE, Arlington, VA. pp. 320–330.

Burcharth, H., Liu, Z., 1995. Rubble mound breakwater failure modes. In: Proceedings of the Final (MAS2 CT92-0042) Workshop: Rubble Mound Failure Modes. Sorrento, Italy.

Castillo, C., Castillo, E., Fernández-Canteli, A., Molina, R., Gómez, R., 2012. Stochastic model for damage accumulation in rubble-mound breakwaters based on compatibility conditions and the central limit theorem. J. Waterw. Port Coast. Ocean. Eng. 138 (6), 451–463. http://dx.doi.org/10.1061/(ASCE)WW.1943-5460.0000146.

Chatenet, Q., Remy, E., Gagnon, M., Fouladirad, M., Tahan, A., 2021. Modeling cavitation erosion using non-homogeneous gamma process. Reliab. Eng. Syst. Saf. 213, 107671. http://dx.doi.org/10.1016/j.ress.2021.107671.

Cinlar, E., Bažant, Z.P., Osman, E., 1977. Stochastic process for extrapolating concrete creep. J. Eng. Mech. Div. 103 (6), 1069–1088. http://dx.doi.org/10.1061/JMCEA3.0002298.

CIRIA/CUR/CETMEF, 2007. The Rock Manual: the Use of Rock in Hydraulic Engineering, vol. 683, Ciria.

Ellingwood, B.R., Mori, Y., 1993. Probabilistic methods for condition assessment and life prediction of concrete structures in nuclear power plants. Nucl. Eng. Des. 142 (2), 155–166. http://dx.doi.org/10.1016/0029-5493(93)90199-J.

Galland, J.C., 1994. Rubble mound breakwater stability under oblique waves: An experimental study. In: Coastal Engineering 1994. pp. 1061–1074. http://dx.doi.org/10.1061/9780784400890.078.

Genest, C., Favre, A.C., 2007. Everything you always wanted to know about copula modeling but were afraid to ask. J. Hydrol. Eng. 12 (4), 347–368. http://dx.doi.org/10.1061/(ASCE)1084-0699(2007)12:4(347).

Golestani, N., Arzaghi, E., Abbassi, R., Garaniya, V., Meng, H., 2023. A system dynamics model of offshore wind farm degradation: Enabling operation and maintenance planning under foreseen asset management impacts. Appl. Ocean Res. 138, 103685. http://dx.doi.org/10.1016/j.apor.2023.103685.

Gómez-Martín, M.E., Medina, J.R., 2006. Damage progression on cube armored breakwaters. Coast. Eng. 5229–5240. http://dx.doi.org/10.1142/9789812709554_0438.

Gómez-Martín, M.E., Medina, J.R., 2014. Heterogeneous packing and hydraulic stability of cube and cubipod armor units. J. Waterw. Port Coast. Ocean. Eng. 140 (1), 100–108. http://dx.doi.org/10.1061/(ASCE)WW.1943-5460.0000223.

Guida, M., Penta, F., 2015. A gamma process model for the analysis of fatigue crack growth data. Eng. Fract. Mech. 142, 21–49. http://dx.doi.org/10.1016/j.engfracmech.2015.05.027.

Hanea, A., Kurowicka, D., Cooke, R., 2006. Hybrid method for quantifying and analyzing Bayesian belief nets. Qual. Reliab. Eng. Int. 22, 709–729. http://dx.doi.org/10.1002/qre.808.

Hanea, A., Morales-Nápoles, O., Ababei, D., 2015. Non-parametric Bayesian networks: Improving theory and reviewing applications. Reliab. Eng. Syst. Saf. 144, 265–284. http://dx.doi.org/10.1016/j.ress.2015.07.027.

Haralambides, H., 2017. Globalization, public sector reform, and the role of ports in international supply chains. Marit. Econ. Logist. 19, 1–51. http://dx.doi.org/10.1057/s41278-017-0068-6.

Henriques, M., Capitão, R., Fortes, C., Lemos, R., Silva, L.G., Silva, H., Gonçalves, R., 2024. The contribution of drones to the monitoring of rubble-mound breakwaters. In: Proceedings of the 10th International Conference on Geographical Information Systems Theory, Applications and Management. GISTAM 2024, SCITPRESS, pp. 160–167. http://dx.doi.org/10.5220/0012691200003696.

Herrera, M.P., Gómez-Martín, M.E., Medina, J.R., 2017. Hydraulic stability of rock armors in breaking wave conditions. Coast. Eng. 127, 55–67. http://dx.doi.org/10.1016/j.coastaleng.2017.06.010.

Hudson, R.Y., 1959. Laboratory investigation of rubble-mound breakwaters. J. Waterw. Harb. Div. 85 (3), 93–121. http://dx.doi.org/10.1061/JWHEAU.0000142.

IPCC, 2023. Weather and climate extreme events in a changing climate. In: Climate Change 2021 – The Physical Science Basis: Working Group I Contribution to the Sixth Assessment Report of the Intergovernmental Panel on Climate Change. Cambridge University Press, pp. 1513–1766. http://dx.doi.org/10.1017/9781009157896.013.

Jumelet, D., van Gent, M.R.A., Hofland, B., Kuiper, C., 2024. Stability of rock-armoured mild slopes. Coast. Eng. 187, 104418. http://dx.doi.org/10.1016/j.coastaleng.2023.104418.

Kolmogorov, A., 1933. Sulla determinazione empirica di una legge di distribuzione. G. Dell'Istituto Ital. Degli Attuari 4, 83–91.

Koot, P., Mendoza-Lugo, M.A., Paprotny, D., Morales-Nápoles, O., Ragno, E., Worm, D.T., 2023. Pybanshee version (1.0): A python implementation of the MATLAB toolbox BANSHEE for non-parametric Bayesian networks with updated features. SoftwareX 21, 101279. http://dx.doi.org/10.1016/j.softx.2022.101279.

Lira-Loarca, A., Cobos, M., Losada, M.Á., Baquerizo, A., 2020. Storm characterization and simulation for damage evolution models of maritime structures. Coast. Eng. 156, 103620. http://dx.doi.org/10.1016/j.coastaleng.2019.103620.

Losada, M.A., Desire, J.M., Alejo, L.M., 1986. Stability of blocks as breakwater armor units. J. Struct. Eng. 112 (11), 2392–2401. http://dx.doi.org/10.1061/(ASCE)0733-9445(1986)112:11(2392).

Lucio, D., Lara, J., Tomás, A., Losada, I., 2024. Projecting compound wave and sea-level events at a coastal structure site under climate change. Coast. Eng. 189, 104490. http://dx.doi.org/10.1016/j.coastaleng.2024.104490.

Mares-Nasarre, P., 2025. Probabilistic estimation of the mean wave overtopping discharge on mound breakwaters. Coast. Eng. 201, 104792. http://dx.doi.org/10.1016/j.coastaleng.2025.104792.

Mares-Nasarre, P., Argente, G., Gómez-Martín, M.E., Medina, J.R., 2021. Armor damage of overtopped mound breakwaters in depth-limited breaking wave conditions. J. Mar. Sci. Eng. 9 (9), http://dx.doi.org/10.3390/jmse9090952.

Mares-Nasarre, P., Molines, J., Gómez-Martín, M.E., Medina, J.R., 2022. Hydraulic stability of cube-armored mound breakwaters in depth-limited breaking wave conditions. Ocean Eng. 259, 111845. http://dx.doi.org/10.1016/j.oceaneng.2022.111845.

Mares-Nasarre, P., Morales-Nápoles, O., Melling, G., 2024a. Armor damage on groins under ship wave attack using field data. In: Proceedings of the 38th Internnational Conference on Coastal Engineering. Rome (Italy). http://dx.doi.org/10.9753/icce.v38.structures.9.

Mares-Nasarre, P., van Gent, M.R.A., Morales-Nápoles, O., 2024b. A copula-based model to describe the uncertainty of overtopping variables on mound breakwaters. Coast. Eng. 189, 104483. http://dx.doi.org/10.1016/j.coastaleng.2024.104483.

Martín-Hidalgo, M., Martín-Soldevilla, M.J., Negro, V., Aberturas, P., López-Gutiérrez, J., 2014. Storm evolution characterization for analysing stone armour damage progression. Coast. Eng. 85, 1–11. http://dx.doi.org/10.1016/j.coastaleng.2013.11.008.

Marzeddu, A., Oliveira, T.C., Sánchez-Arcilla, A., Gironella, X., 2020. Effect of wave storm representation on damage measurements of breakwaters. Ocean Eng. 200, 107082. http://dx.doi.org/10.1016/j.oceaneng.2020.107082.

Medina, J., 2024. Breakwaters in a living environment. CoastLab 2024: Phys. Model. Coast. Eng. Sci. http://dx.doi.org/10.59490/coastlab.2024.819.

Melby, J., Kobayashi, N., 1999. Damage progression and variability on breakwater trunks. Coast. Struct. 309–316.

Mendoza-Lugo, M.A., Delgado-Hernández, D.J., Morales-Nápoles, O., 2019. Reliability analysis of reinforced concrete vehicle bridges columns using non-parametric Bayesian networks. Eng. Struct. 188, 178–187. http://dx.doi.org/10.1016/j.engstruct.2019.03.011.

Mendoza-Lugo, M.A., Morales-Nápoles, O., Delgado-Hernández, D.J., 2022. A non-parametric Bayesian network for multivariate probabilistic modelling of weigh-in-motion system data. Transp. Res. Interdiscip. Perspect. 13, 100552. http://dx.doi.org/10.1016/j.trip.2022.100552.

Morales-Nápoles, O., Hanea, A., Worm, D., 2013a. Experimental Results About the Assessments of Conditional Rank Correlations by Experts: Example with Air Pollution Estimates. Taylor & Francis Group, pp. 1359–1366. http://dx.doi.org/10.1201/b15938-204.

Morales-Nápoles, O., Hanea, A.M., Worm, D.T.H., 2013b. Experimental results about the assessments of conditional rank correlations by experts: Example with air pollution estimates. In: ESREL 2013. http://dx.doi.org/10.1201/b15938-204.

Musumeci, R.E., Moltisanti, D., Foti, E., Battiato, S., Farinella, G.M., 2018. 3-D monitoring of rubble mound breakwater damages. Measurement 117, 347–364. http://dx.doi.org/10.1016/j.measurement.2017.12.020.

Nørgaard, J.Q.H., Lykke Andersen, T., Burcharth, H.F., 2014. Distribution of individual wave overtopping volumes in shallow water wave conditions. Coast. Eng. 83, 15–23. http://dx.doi.org/10.1016/j.coastaleng.2013.09.003.

Norris, J.R., 1997. Markov chains. In: Cambridge Series in Statistical and Probabilistic Mathematics, Cambridge University Press.

Paprotny, D., 't Hart, C.M.P., Morales-Nápoles, O., 2024. Evolution of flood protection levels and flood vulnerability in Europe since 1950 estimated with vine-copula models. Nat. Hazards 121 (5), 6155–6184. http://dx.doi.org/10.1007/s11069-024-07039-5.

Puente, I., Sande, J., González-Jorge, H., Peña-González, E., Maciñeira, E., Martínez-Sánchez, J., Arias, P., 2014. Novel image analysis approach to the terrestrial LiDAR monitoring of damage in rubble mound breakwaters. Ocean Eng. 91, 273–280. http://dx.doi.org/10.1016/j.oceaneng.2014.09.011.

Puertos del Estado, 2012. Diques de abrigo en los puertos de interés general del Estado: años 1986–2011. Organismo Público Puertos del Estado.

Puertos del Estado, 2024. Conjunto de datos: REDCOS. Minist. Transp. Y Movil. Sosten. URL: https://bancodatos.puertos.es/BD/informes/INT_1.pdf.

Rongen, G., Morales-Nápoles, O., 2024. Matlatzinca: A PyBANSHEE-based graphical user interface for elicitation of non-parametric Bayesian networks from experts. SoftwareX 26, 101693. http://dx.doi.org/10.1016/j.softx.2024.101693.

Rongen, G., Morales-Nápoles, O., Worm, D., Kok, M., 2025. Structured expert elicitation of dependence between river tributaries using nonparametric Bayesian networks. Risk Anal. http://dx.doi.org/10.1111/risa.70111, URL: https://onlinelibrary.wiley.com/doi/abs/10.1111/risa.70111.

Sande, J., Peña, E., Maciñeira, E., 2018. Stability of breakwater roundhead protected with a cubipod single-layer armor. Appl. Ocean Res. 79, 36–48. http://dx.doi.org/10.1016/j.apor.2018.07.006.

Scaravaglione, G., Marino, S., Francone, A., Leone, E., Damiani, L., Tomasicchio, G.R., van Gent, M.R.A., Saponieri, A., 2025a. The influence of shallow water on rock armour stability. Coast. Eng. 197, 104657. http://dx.doi.org/10.1016/j.coastaleng.2024.104657.

Scaravaglione, G., Melby, J.A., Tomasicchio, G.R., van Gent, M.R.A., Saponieri, A., 2025b. On the uncertainties in stone armor stability. Coast. Eng. 104790. http://dx.doi.org/10.1016/j.coastaleng.2025.104790.

Sebastian, A., Dupuits, E., Morales-Nápoles, O., 2017. Applying a Bayesian network based on Gaussian copulas to model the hydraulic boundary conditions for hurricane flood risk analysis in a coastal watershed. Coast. Eng. 125, 42–50. http://dx.doi.org/10.1016/j.coastaleng.2017.03.008.

Sklar, M., 1959. Fonctions de repartition a n dimensions et leurs marges. Publ. Inst. Stat. Univ. Paris 8, 229–231, URL: https://hal.science/hal-04094463/document.

Smirnov, N., 1949. Table for estimating the goodness of fit of empirical distributions. Ann. Math. Stat. 19 (2), 279–281. http://dx.doi.org/10.1214/aoms/1177730256.

Spearman, C., 1904. The proof and measurement of association between two things. Am. J. Psychol. 15 (1), 72–101.

Straub, D., 2009. Stochastic modeling of deterioration processes through dynamic Bayesian networks. J. Eng. Mech. (ASCE) 135, http://dx.doi.org/10.1061/(ASCE)EM.1943-7889.0000024.

USACE, 1984. Shore Protection Manual. U.S. Army Coastal Engineering Research Center. U.S. Army Engineer Waterways Experiment Station, Vicksburg, Mississipi.

USACE, 2002. CEM: Coastal Engineering Manual. U.S. Army Corps of Engineers, URL: https://books.google.nl/books?id=QLO_jwEACAAJ.

van der Meer, J.W., 1987. Stability of breakwater armour layers — design formulae. Coast. Eng. 11 (3), 219–239. http://dx.doi.org/10.1016/0378-3839(87)90013-5.

van der Meer, J.W., 1988. Rock Slopes and Gravel Beaches Under Wave Attack (Ph.D. thesis). Delft Hydraulics, Netherlands.

van Gent, M.R.A., 2014. Oblique wave attack on rubble mound breakwaters. Coast. Eng. 88, 43–54. http://dx.doi.org/10.1016/j.coastaleng.2014.02.002.

van Gent, M.R.A., Smale, A.J., Kuiper, C., 2003. Stability of rock slopes with shallow foreshores. In: Coastal Structures 2003 - Proceedings of the Conference. http://dx.doi.org/10.1061/40733(147)9.

van Noortwijk, J., 2009. A survey of the application of gamma processes in maintenance. Reliab. Eng. Syst. Saf. 94 (1), 2–21. http://dx.doi.org/10.1016/j.ress.2007.03.019, Maintenance Modeling and Application.

van Noortwijk, J., Klatter, H., 1999. Optimal inspection decisions for the block mats of the Eastern-Scheldt barrier. Reliab. Eng. Syst. Saf. 65 (3), 203–211. http://dx.doi.org/10.1016/S0951-8320(98)00097-0.

Vidal, C., Losada, M.A., Medina, R., 1991. Stability of mound breakwater's head and trunk. J. Waterw. Port Coast. Ocean. Eng. 117 (6), 570–587. http://dx.doi.org/10.1061/(ASCE)0733-950X(1991)117:6(570).

Vousdoukas, M., Mentaschi, L., Voukouvalas, E., Verlaan, M., Jevrejeva, S., Jackson, L., Feyen, L., 2018. Global probabilistic projections of extreme sea levels show intensification of coastal flood hazard. Nat. Commun. 9, http://dx.doi.org/10.1038/s41467-018-04692-w.

Wolters, G., van Gent, M.R.A., 2011. Oblique wave attack on cube and rock armoured rubble mound breakwaters. Coast. Eng. Proc. 1 (32), http://dx.doi.org/10.9753/icce.v32.structures.34, structures.34.

Yuksel, Y., Cevik, E., Sahin, C., van Gent, M.R.A., Gumus, S., Issever, D., Inal, U., Ogur, M.U., 2025. Structural and hydraulic response of emerged low-crested cube-armoured breakwaters. Appl. Ocean Res. 156, 104488. http://dx.doi.org/10.1016/j.apor.2025.104488.

Yuksel, Y., Cevik, E., van Gent, M.R.A., Sahin, C., Altunsu, A., Tugce Yuksel, Z., 2020. Stability of berm type breakwater with cube blocks in the lower slope and berm. Ocean Eng. 217, 107985. http://dx.doi.org/10.1016/j.oceaneng.2020.107985.

Yuksel, Y., van Gent, M.R., Cevik, E., Kaya, A.H., Ari Guner, H.A., Yuksel, Z.T., Gumuscu, I., 2022. Stability of high density cube armoured breakwaters. Ocean Eng. 253, 111317. http://dx.doi.org/10.1016/j.oceaneng.2022.111317.